

CHAPTER

7

ANTENNA SYNTHESIS AND CONTINUOUS SOURCES

7.1 INTRODUCTION

Thus far in the book we have concentrated primarily on the analysis and design of antennas. In the analysis problem an antenna model is chosen, and it is analyzed for its radiation characteristics (pattern, directivity, impedance, beamwidth, efficiency, polarization, and bandwidth). This is usually accomplished by initially specifying the current distribution of the antenna, and then analyzing it using standard procedures. If the antenna current is not known, it can usually be determined from integral equation formulations. Numerical techniques, such as the Moment Method of Chapter 8, can be used to numerically solve the integral equations.

In practice, it is often necessary to design an antenna system that will yield desired radiation characteristics. For example, a very common request is to design an antenna whose far-field pattern possesses nulls in certain directions. Other common requests are for the pattern to exhibit a desired distribution, narrow beamwidth and low side lobes, decaying minor lobes, and so forth. The task, in general, is to find not only the antenna configuration but also its geometrical dimensions and excitation distribution. The designed system should yield, either exactly or approximately, an acceptable radiation pattern, and it should satisfy other system constraints. This method of design is usually referred to as *synthesis*. Although synthesis, in its broadest definition, usually refers to antenna pattern synthesis, it is often used interchangeably with design. Since design methods have been outlined and illustrated previously, in this chapter we want to introduce and illustrate antenna pattern synthesis methods.

Antenna pattern synthesis usually requires that first an approximate analytical model is chosen to represent, either exactly or approximately, the desired pattern. The second step is to realize the analytical model by an antenna model. Generally speaking, antenna pattern synthesis can be classified into three categories. One group requires that the antenna patterns possess nulls in desired directions. The method introduced by Schelkunoff [1] can be used to accomplish this; it will be discussed in Section 7.3. Another category requires that the patterns exhibit a desired distribution in the entire visible region. This is referred to as *beam shaping*, and it can be accomplished using the Fourier transform [2] and the Woodward-Lawson [3], [4] methods. They will be discussed and illustrated in Sections 7.4 and 7.5, respectively. A third group includes

techniques that produce patterns with narrow beams and low side lobes. Some methods that accomplish this have already been discussed: namely the binomial method (Section 6.8.2) and the Dolph-Tschebyscheff method (also spelled Tchebyscheff or Chebyshev) of Section 6.8.3. Other techniques that belong to this family are the Taylor line-source (Tschebyscheff error) [5] and the Taylor line-source (one-parameter) [6]. They will be outlined and illustrated in Sections 7.6 and 7.7, respectively.

The synthesis methods will be utilized to design line-sources and linear arrays whose space factors [as defined by (4-58a)] and array factors [as defined by (6-52)] will yield desired far-field radiation patterns. The total pattern is formed by multiplying the space factor (or array factor) by the element factor (or element pattern) as dictated by (4-59) [or (6-5)]. For very narrow beam patterns, the total pattern is nearly the same as the space factor or array factor. This is demonstrated by the dipole antenna ($l \leq \lambda$) of Figure 4.5 whose element factor, as given by (4-58a), is $\sin \theta$; for values of θ near 90° ($\theta \approx 90^\circ$), $\sin \theta \approx 1$.

The synthesis techniques will be followed with a brief discussion of some very popular line-source distributions (triangular, cosine, cosine-squared) and continuous aperture distributions (rectangular and circular).

7.2 CONTINUOUS SOURCES

Very long (in terms of a wavelength) arrays of discrete elements usually are more difficult to implement, more costly, and have narrower bandwidths. For such applications, antennas with continuous distributions would be convenient to use. A very long wire and a large reflector represent, respectively, antennas with continuous line and aperture distributions. Continuous distribution antennas usually have larger side lobes, are more difficult to scan, and in general, they are not as versatile as arrays of discrete elements. The characteristics of continuously distributed sources can be approximated by discrete-element arrays, and vice-versa, and their development follows and parallels that of discrete-element arrays.

7.2.1 Line-Source

Continuous line-source distributions are functions of only one coordinate, and they can be used to approximate linear arrays of discrete elements and vice-versa.

The array factor of a discrete-element array, placed along the z -axis, is given by (6-52) and (6-52a). As the number of elements increases in a fixed-length array, the source approaches a continuous distribution. In the limit, the array factor summation reduces to an integral. For a continuous distribution, the factor that corresponds to the array factor is known as the *space factor*. For a line-source distribution of length l placed symmetrically along the z -axis as shown in Figure 7.1(a), the space factor (SF) is given by

$$\text{SF}(\theta) = \int_{-l/2}^{+l/2} I_n(z') e^{j[kz' \cos \theta + \phi_n(z')] } dz' \quad (7-1)$$

where $I_n(z')$ and $\phi_n(z')$ represent, respectively, the amplitude and phase distributions along the source. For a constant phase distribution $\phi_n(z') = 0$.

Equation (7-1) is a finite one-dimensional Fourier transform relating the far-field pattern of the source to its excitation distribution. Two-dimensional Fourier transforms are used to represent the space factors for two-dimensional source distributions. These relations are results of the angular spectrum concept for plane waves, introduced first

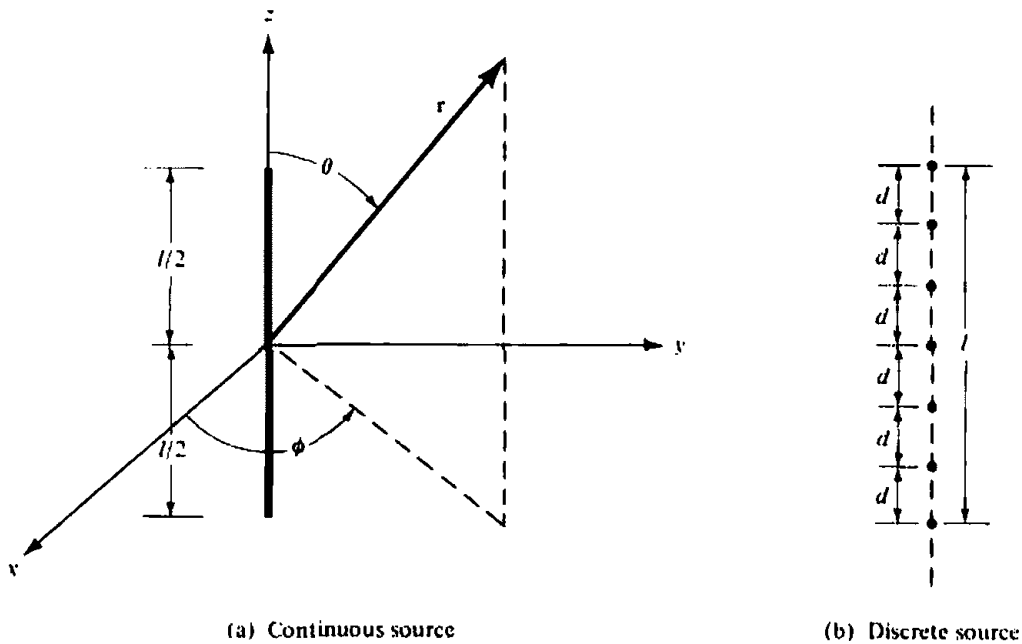


Figure 7.1 Continuous and discrete linear sources.

by Booker and Clemmow [2], and it relates the angular spectrum of a wave to the excitation distribution of the source.

For a continuous source distribution, the total field is given by the product of the *element* and *space* factors as defined in (4-59). This is analogous to the pattern multiplication of (6-5) for arrays. *The type of current and its direction of flow on a source determine the element factor.* For a finite length linear dipole, for example, the total field of (4-58a) is obtained by summing the contributions of small infinitesimal elements which are used to represent the entire dipole. In the limit, as the infinitesimal lengths become very small, the summation reduces to an integration. In (4-58a), the factor outside the brackets is the element factor and the one within the brackets is the space factor and corresponds to (7-1).

7.2.2 Discretization of Continuous Sources

The radiation characteristics of continuous sources can be approximated by discrete-element arrays, and vice-versa. This is illustrated in Figure 7.1(b) whereby discrete elements, with a spacing d between them, are placed along the length of the continuous source. Smaller spacings between the elements yield better approximations, and they can even capture the fine details of the continuous distribution radiation characteristics. For example, the continuous line-source distribution $I_n(z')$ of (7-1) can be approximated by a discrete-element array whose element excitation coefficients, at the specified element positions within $-l/2 \leq z' \leq l/2$, are determined by the sampling of $I_n(z')e^{j\phi_n(z')}$. The radiation pattern of the digitized discrete-element array will approximate the pattern of the continuous source.

The technique can be used for the discretization of any continuous distribution. The accuracy increases as the element spacing decreases; in the limit, the two patterns will be identical. For large element spacing, the patterns of the two antennas will not match well. To avoid this, another method known as *root-matching* can be used [7]. Instead of sampling the continuous current distribution to determine the element excitation coefficients, the root-matching method requires that the nulls of the contin-

uous distribution pattern also appear in the initial pattern of the discrete-element array. If the synthesized pattern using this method still does not yield (within an acceptable accuracy) the desired pattern, a perturbation technique [7] can then be applied to the distribution of the discrete-element array to improve its accuracy.

7.3 SCHELKUNOFF POLYNOMIAL METHOD

A method that is conducive to the synthesis of arrays whose patterns possess nulls in desired directions is that introduced by Schelkunoff [1]. To complete the design, this method requires information on the number of nulls and their locations. The number of elements and their excitation coefficients are then derived. The analytical formation of the technique follows.

Referring to Figure 6.5(a), the array factor for an N -element, equally spaced, nonuniform amplitude, and progressive phase excitation is given by (6-52) as

$$\text{AF} = \sum_{n=1}^N a_n e^{j(n-1)(kd \cos \theta + \beta)} = \sum_{n=1}^N a_n e^{j(n-1)\psi} \quad (7-2)$$

where a_n accounts for the nonuniform amplitude excitation of each element. The spacing between the elements is d and β is the progressive phase shift.

Letting

$$z = x + jy = e^{j\psi} = e^{jkd \cos \theta + \beta} \quad (7-3)$$

we can rewrite (7-2) as

$$\text{AF} = \sum_{n=1}^N a_n z^{n-1} = a_1 + a_2 z + a_3 z^2 + \cdots + a_N z^{N-1} \quad (7-4)$$

which is a polynomial of degree $(N - 1)$. From the mathematics of complex variables and algebra, any polynomial of degree $(N - 1)$ has $(N - 1)$ roots and can be expressed as a product of $(N - 1)$ linear terms. Thus we can write (7-4) as

$$\text{AF} = a_n (z - z_1)(z - z_2)(z - z_3) \cdots (z - z_{N-1}) \quad (7-5)$$

where $z_1, z_2, z_3, \dots, z_{N-1}$ are the roots, which may be complex, of the polynomial. The magnitude of (7-5) can be expressed as

$$|\text{AF}| = |a_n| |z - z_1| |z - z_2| |z - z_3| \cdots |z - z_{N-1}| \quad (7-6)$$

Some very interesting observations can be drawn from (7-6) which can be used judiciously for the analysis and synthesis of arrays. Before tackling that phase of the problem, let us first return and examine the properties of (7-3).

The complex variable z of (7-3) can be written in another form as

$$z = |z| e^{j\psi} = |z| \angle \psi = 1 \angle \psi \quad (7-7)$$

$$\psi = kd \cos \theta + \beta = \frac{2\pi}{\lambda} d \cos \theta + \beta \quad (7-7a)$$

It is clear that for any value of d , θ , or β the magnitude of z lies always on a *unit* circle; however its phase depends upon d , θ , and β . For $\beta = 0$, we have plotted in Figures 7-2(a)–(d) the value of z , magnitude and phase, as θ takes values of 0 to π rad. It is observed that for $d = \lambda/8$ the values of z , for all the physically observable

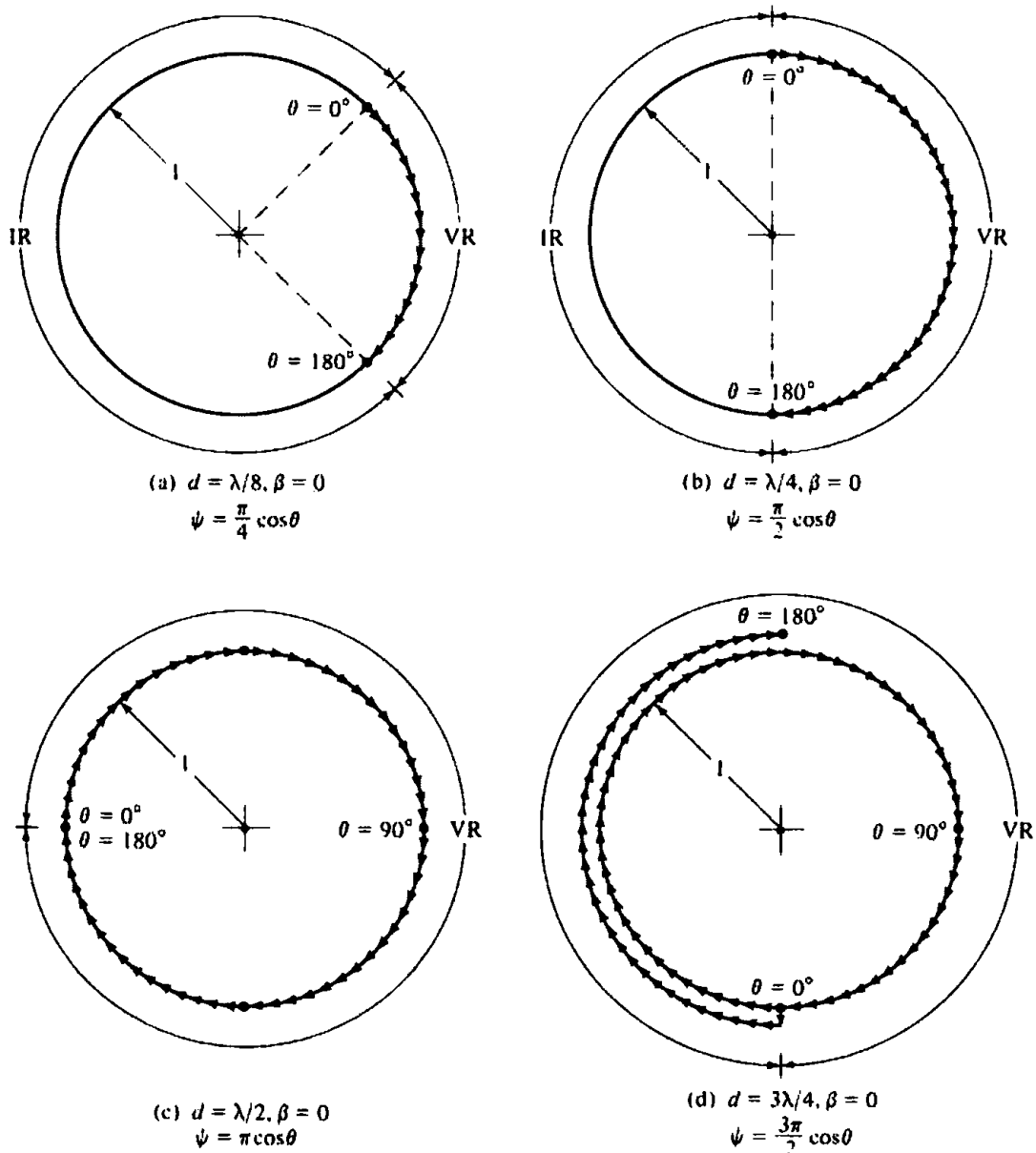


Figure 7.2 Visible Region (VR) and Invisible Region (IR) boundaries for complex variable z when $\beta = 0$.

angles of θ , only exist over the part of the circle shown in Figure 7.2(a). Any values of z outside that arc are not realizable by any observation angle θ for the spacing $d = \lambda/8$. We refer to the realizable part of the circle as the *visible region* and the remaining as the *invisible region*. In Figure 7.2(a) we also observe the path of the z values as θ changes from 0° to 180° .

In Figures 7.2(b)–(d) we have plotted the values of z when the spacing between the elements is $\lambda/4$, $\lambda/2$, and $3\lambda/4$. It is obvious that the visible region can be extended by increasing the spacing between the elements. It requires a spacing of at least $\lambda/2$ to encompass, at least once, the entire circle. Any spacing greater than $\lambda/2$ leads to multiple values for z . In Figure 7.2(d) we have double values for z for half of the circle when $d = 3\lambda/4$.

To demonstrate the versatility of the arrays, in Figures 7.3(a)–(d) we have plotted the values of z for the same spacings as in Figures 7.2(a)–(d) but with a $\beta = \pi/4$. A comparison between the corresponding figures indicates that the overall visible region

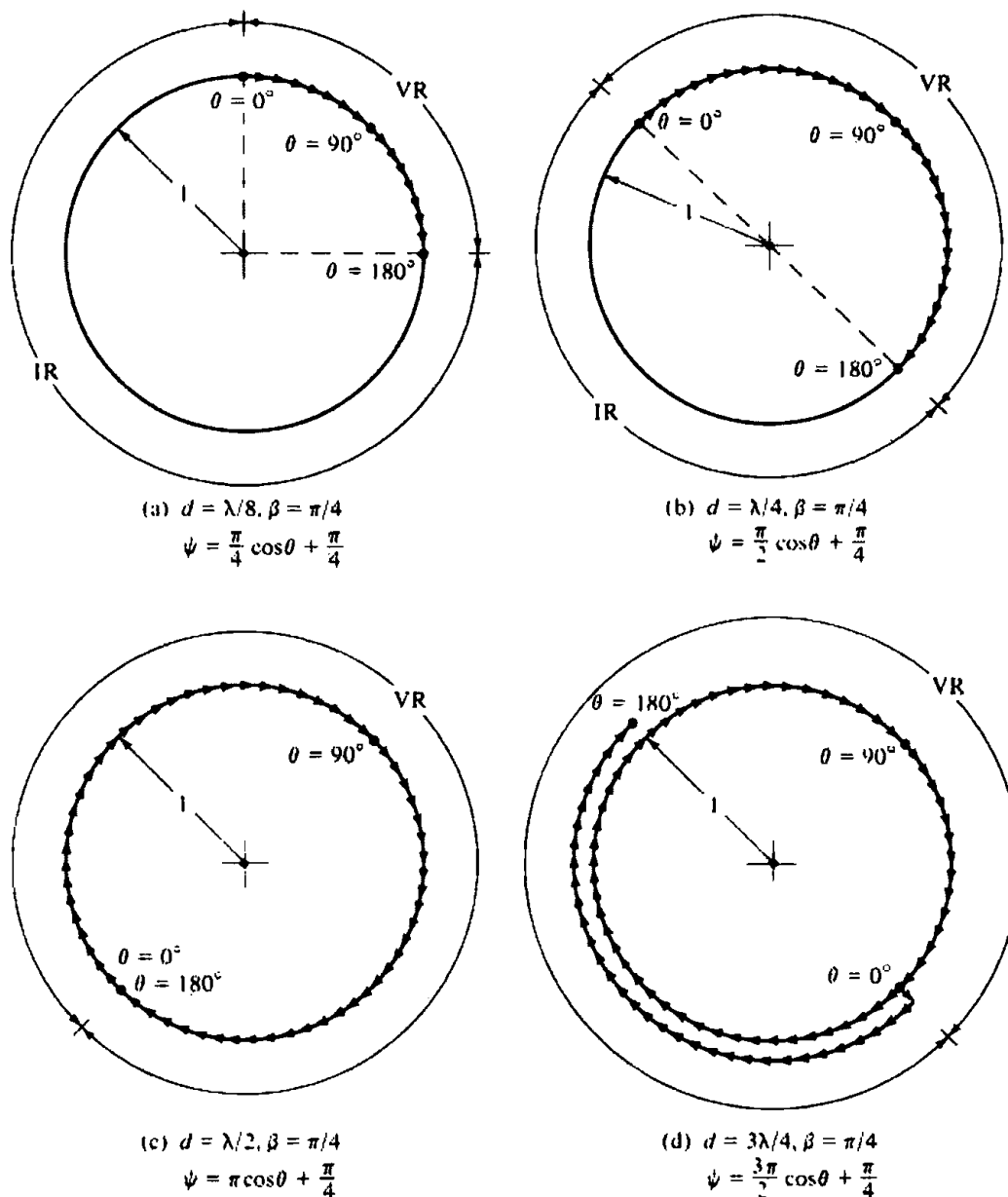


Figure 7.3 Visible Region (VR) and Invisible Region (IR) boundaries for complex variable z when $\beta = \pi/4$.

for each spacing has not changed but its relative position on the circle has rotated counterclockwise by an amount equal to β .

We can conclude then that the overall extent of the visible region can be controlled by the spacing between the elements and its relative position on the circle by the progressive phase excitation of the elements. These two can be used effectively in the design of the array factors.

Now let us return to (7-6). The magnitude of the array factor, its form as shown in (7-6), has a geometrical interpretation. For a given value of z in the visible region of the unit circle, corresponding to a value of θ as determined by (7-3), $|AF|$ is proportional to the product of the distances between z and $z_1, z_2, z_3, \dots, z_{N-1}$, the roots of AF. In addition, apart from a constant, the phase of AF is equal to the sum of the phases between z and each of the zeros (roots). This is best demonstrated geometrically in Figure 7.4(a). If all the roots $z_1, z_2, z_3, \dots, z_{N-1}$ are located in the visible region of the unit circle, then each one corresponds to a null in the pattern of

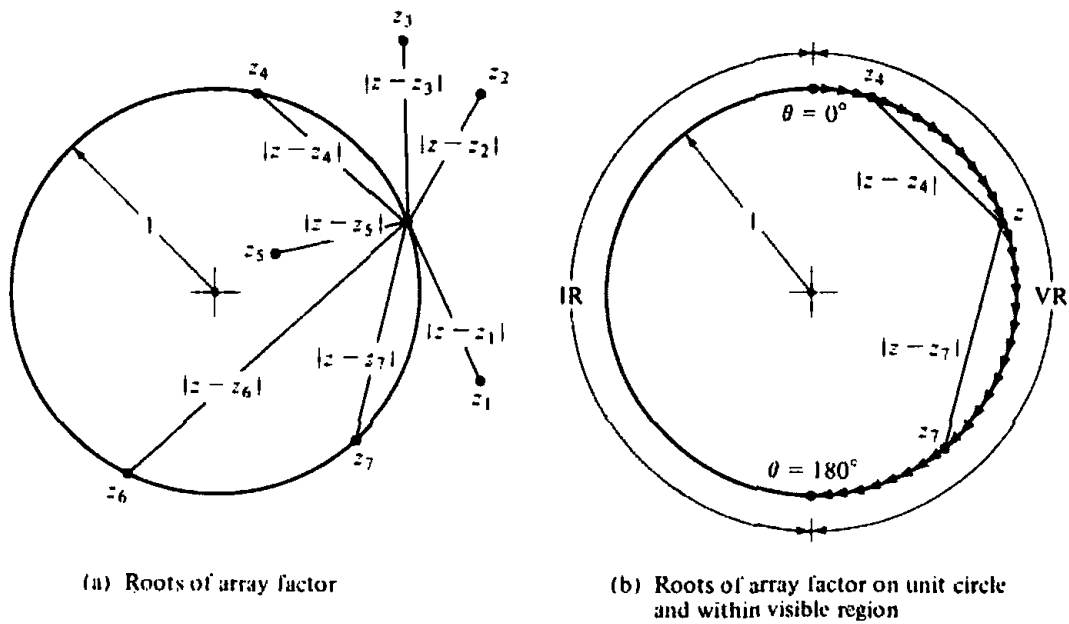


Figure 7.4 Array factor roots within and outside unit circle, and visible and invisible regions.

$|AF|$ because as θ changes z changes and eventually passes through each of the z_n 's. When it does, the length between z and that z_n is zero and (7-6) vanishes. When all the zeros (roots) are not in the visible region of the unit circle, but some lie outside it and/or any other point not on the unit circle, then only those zeros on the visible region will contribute to the nulls of the pattern. This is shown geometrically in Figure 7.4(b). If no zeros exist in the visible region of the unit circle, then that particular array factor has no nulls for any value of θ . However, if a given zero lies on the unit circle but not in its visible region, that zero can be included in the pattern by changing the phase excitation β so that the visible region is rotated until it encompasses that root. Doing this, and not changing d , may exclude some other zero(s).

To demonstrate all the principles, we will consider an example along with some computations.

Example 7.1

Design a linear array with a spacing between the elements of $d = \lambda/4$ such that it has zeros at $\theta = 0^\circ, 90^\circ,$ and 180° . Determine the number of elements, their excitation, and plot the derived pattern. Use Schelkunoff's method.

SOLUTION

For a spacing of $\lambda/4$ between the elements and a phase shift $\beta = 0^\circ$, the visible region is shown in Figure 7.2(b). If the desired zeros of the array factor must occur at $\theta = 0^\circ, 90^\circ,$ and 180° , then these correspond to $z = j, 1, -j$ on the unit circle. Thus a normalized form of the array factor is given by

$$AF = (z - z_1)(z - z_2)(z - z_3) = (z - j)(z - 1)(z + j)$$

$$AF = z^3 - z^2 + z - 1$$

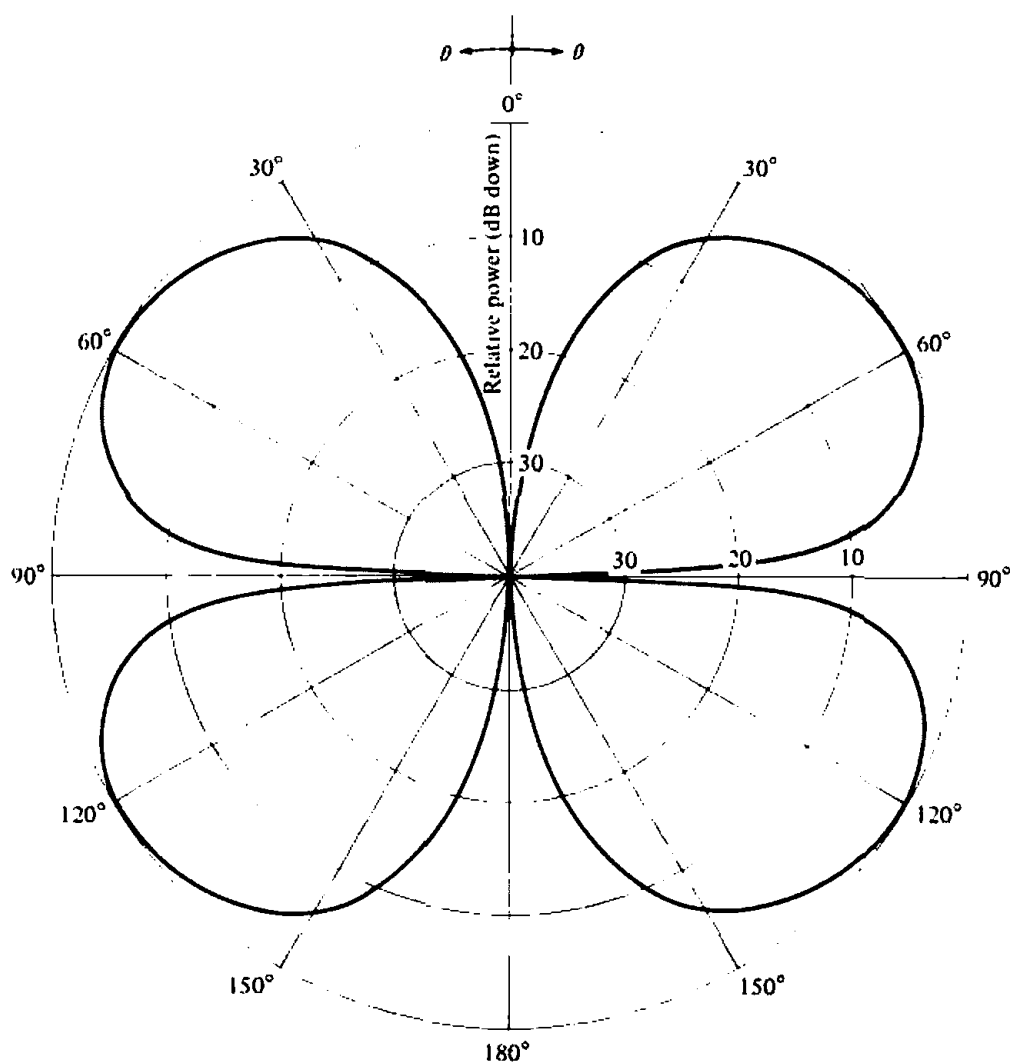


Figure 7.5 Amplitude radiation pattern of a four-element array of isotropic sources with a spacing of $\lambda/4$ between them, zero degrees progressive phase shift, and zeros at $\theta = 0^\circ, 90^\circ,$ and 180° .

Referring to (7-4), the above array factor and the desired radiation characteristics can be obtained when there are four elements and their excitation coefficients are equal to

$$a_1 = -1$$

$$a_2 = +1$$

$$a_3 = -1$$

$$a_4 = +1$$

To illustrate the method, we plotted in Figure 7.5 the pattern of that array; it clearly meets the desired specifications. Because of the symmetry of the array, the pattern of the left hemisphere is identical to that of the right.

7.4 FOURIER TRANSFORM METHOD

This method can be used to determine, given a complete description of the desired pattern, the excitation distribution of a continuous or a discrete source antenna system.

The derived excitation will yield, either exactly or approximately, the desired antenna pattern. The pattern synthesis using this method is referred to as *beam shaping*.

7.4.1 Line-Source

For a continuous line-source distribution of length l , as shown in Figure 7.1, the normalized space factor of (7-1) can be written as

$$\text{SF}(\theta) = \int_{-l/2}^{l/2} I(z') e^{jk \cos \theta - k_z z'} dz' = \int_{-l/2}^{l/2} I(z') e^{j\xi z'} dz' \quad (7-8)$$

$$\xi = k \cos \theta - k_z \Rightarrow \theta = \cos^{-1} \left(\frac{\xi + k_z}{k} \right) \quad (7-8a)$$

where k_z is the excitation phase constant of the source. For a normalized uniform current distribution of the form $I(z') = I_0/l$, (7-8) reduces to

$$\text{SF}(\theta) = I_0 \frac{\sin \left[\frac{kl}{2} \left(\cos \theta - \frac{k_z}{k} \right) \right]}{\frac{kl}{2} \left(\cos \theta - \frac{k_z}{k} \right)} \quad (7-9)$$

The observation angle θ of (7-9) will have real values (visible region) provided that $-(k + k_z) \leq \xi \leq (k - k_z)$ as obtained from (7-8a).

Since the current distribution of (7-8) extends only over $-l/2 \leq z' \leq l/2$ (and it is zero outside it), the limits can be extended to infinity and (7-8) can be written as

$$\text{SF}(\theta) = \text{SF}(\xi) = \int_{-\infty}^{+\infty} I(z') e^{j\xi z'} dz' \quad (7-10a)$$

The form of (7-10a) is a Fourier transform, and it relates the excitation distribution $I(z')$ of a continuous source to its far-field space factor $\text{SF}(\theta)$. The transform pair of (7-10a) is given by

$$I(z') = \frac{1}{2\pi} \int_{-\infty}^{+\infty} \text{SF}(\xi) e^{-j\xi z'} d\xi = \frac{1}{2\pi} \int_{-\infty}^{+\infty} \text{SF}(\theta) e^{-j\xi z'} d\xi \quad (7-10b)$$

Whether (7-10a) represents the direct transform and (7-10b) the inverse transform, or vice-versa, does not matter here. The most important thing is that the excitation distribution and the far-field space factor are related by Fourier transforms.

Equation (7-10b) indicates that if $\text{SF}(\theta)$ represents the desired pattern, the excitation distribution $I(z')$ that will yield the exact desired pattern must in general exist for all values of z' ($-\infty \leq z' \leq \infty$). Since physically only sources of finite dimensions are realizable, the excitation distribution of (7-10b) is truncated at $z' = \pm l/2$ (beyond $z' = \pm l/2$ it is set to zero). Thus the approximate source distribution is given by

$$I_a(z') = \begin{cases} I(z') = \frac{1}{2\pi} \int_{-\infty}^{+\infty} \text{SF}(\xi) e^{-j\xi z'} d\xi & -l/2 \leq z' \leq l/2 \\ 0 & \text{elsewhere} \end{cases} \quad (7-11)$$

and it yields an approximate pattern $SF(\theta)_a$. The approximate pattern is used to represent, within certain error, the desired pattern $SF(\theta)_d$. Thus

$$SF(\theta)_d = SF(\theta)_a = \int_{-l/2}^{l/2} I_a(z') e^{j\xi z'} dz' \quad (7-12)$$

It can be shown that, over all values of ξ , the synthesized approximate pattern $SF(\theta)_a$ yields the least mean square error or deviation from the desired pattern $SF(\theta)_d$. However that criterion is not satisfied when the values of ξ are restricted only in the visible region [8], [9].

To illustrate the principles of this design method, an example is taken.

Example 7.2

Determine the current distribution and the approximate radiation pattern of a line-source placed along the z -axis whose desired radiation pattern is symmetrical about $\theta = \pi/2$, and it is given by

$$SF(\theta) = \begin{cases} 1 & \pi/4 \leq \theta \leq 3\pi/4 \\ 0 & \text{elsewhere} \end{cases}$$

This is referred to as a sectoral pattern, and it is widely used in radar search and communication applications.

SOLUTION

Since the pattern is symmetrical, $k_z = 0$. The values of ξ , as determined by (7-8a), are given by $k/\sqrt{2} \geq \xi \geq -k/\sqrt{2}$. In turn, the current distribution is given by (7-10b) or

$$\begin{aligned} I(z') &= \frac{1}{2\pi} \int_{-\infty}^{+\infty} SF(\xi) e^{-jz'\xi} d\xi \\ &= \frac{1}{2\pi} \int_{-k/\sqrt{2}}^{k/\sqrt{2}} e^{-jz'\xi} d\xi = \frac{k}{\pi\sqrt{2}} \left[\frac{\sin\left(\frac{kz'}{\sqrt{2}}\right)}{\frac{kz'}{\sqrt{2}}} \right] \end{aligned}$$

and it exists over all values of z' ($-\infty \leq z' \leq \infty$). Over the extent of the line source, the current distribution is approximated by

$$I_a(z') \approx I(z'), \quad -l/2 \leq z' \leq l/2$$

If the derived current distribution $I(z')$ is used in conjunction with (7-10a) and it is assumed to exist over all values of z' , the exact and desired sectoral pattern will result. If however it is truncated at $z' = \pm l/2$ (and assumed to be zero outside), then the desired pattern is approximated by (7-12) or

$$SF(\theta)_d = SF(\theta)_a = \int_{-l/2}^{l/2} I_a(z') e^{j\xi z'} dz'$$

$$= \frac{1}{\pi} \left\{ S_i \left[\frac{l}{\lambda} \pi \left(\cos \theta + \frac{1}{\sqrt{2}} \right) \right] - S_i \left[\frac{l}{\lambda} \pi \left(\cos \theta - \frac{1}{\sqrt{2}} \right) \right] \right\}$$

where $S_i(x)$ is the sine integral of (4-68b).

The approximate current distribution (normalized so that its maximum is unity) is plotted in Figure 7.6(a) for $l = 5\lambda$ and $l = 10\lambda$. The corresponding approximate normalized patterns are shown in Figure 7.6(b) where they are compared with the desired pattern. A very good reconstruction is indicated. The longer line source ($l = 10\lambda$) provides a better realization. The side lobes are about 0.102 (-19.83 dB) for $l = 5\lambda$ and 0.081 (-21.83 dB) for $l = 10\lambda$ (relative to the pattern at $\theta = 90^\circ$).

7.4.2 Linear Array

The array factor of an N -element linear array of equally spaced elements and non-uniform excitation is given by (7-2). If the reference point is taken at the physical center of the array, the array factor can also be written as

Odd Number of Elements ($N = 2M + 1$)

$$\boxed{\text{AF}(\theta) = \text{AF}(\psi) = \sum_{m=-M}^M a_m e^{jm\psi}} \quad (7-13a)$$

Even Number of Elements ($N = 2M$)

$$\boxed{\text{AF}(\theta) = \text{AF}(\psi) = \sum_{m=-M}^{-1} a_m e^{j(2m-1)/2\psi} + \sum_{m=1}^M a_m e^{j(2m-1)/2\psi}} \quad (7-13b)$$

where

$$\boxed{\psi = kd \cos \theta + \beta} \quad (7-13c)$$

For an odd number of elements ($N = 2M + 1$), the elements are placed at

$$z'_m = md, \quad m = 0, \pm 1, \pm 2, \dots, \pm M \quad (7-13d)$$

and for an even number ($N = 2M$) at

$$z'_m = \begin{cases} \frac{2m-1}{2}d, & 1 \leq m \leq M \\ \frac{2m+1}{2}d, & -M \leq m \leq -1 \end{cases} \quad (7-13e)$$

An odd number of elements must be utilized to synthesize a desired pattern whose average value, over all angles, is not equal to zero. The $m = 0$ term of (7-13a) is analogous to the d.c. term in a Fourier series expansion of functions whose average value is not zero.

In general, the array factor of an antenna is a periodic function of ψ , and it must repeat for every 2π radians. In order for the array factor to satisfy the periodicity requirements for real values of θ (visible region), then $2kd = 2\pi$ or $d = \lambda/2$. The periodicity and visible region requirement of $d = \lambda/2$ can be relaxed; in fact, it can be made $d < \lambda/2$. However, the array factor $\text{AF}(\psi)$ must be made pseudoperiodic by using fill-in functions, as is customarily done in Fourier series analysis. Such a

construction leads to nonunique solutions, because each new fill-in function will result in a different solution. In addition, spacings smaller than $\lambda/2$ lead to superdirective arrays that are undesirable and impractical. If $d > \lambda/2$, the derived patterns exhibit undesired grating lobes; in addition, they must be restricted to satisfy the periodicity requirements.

If $AF(\psi)$ represents the desired array factor, the excitation coefficients of the array can be obtained by the Fourier formula of

Odd Number of Elements ($N = 2M + 1$)

$$a_m = \frac{1}{T} \int_{-T/2}^{T/2} AF(\psi) e^{-jm\psi} d\psi = \frac{1}{2\pi} \int_{-\pi}^{\pi} AF(\psi) e^{-jm\psi} d\psi \quad -M \leq m \leq M \quad (7-14a)$$

Even Number of Elements ($N = 2M$)

$$a_m = \begin{cases} \frac{1}{T} \int_{-T/2}^{T/2} AF(\psi) e^{-j(2m+1/2)\psi} d\psi \\ \quad = \frac{1}{2\pi} \int_{-\pi}^{\pi} AF(\psi) e^{-j(2m+1/2)\psi} d\psi & -M \leq m \leq -1 \\ \frac{1}{T} \int_{-T/2}^{T/2} AF(\psi) e^{j(2m-1/2)\psi} d\psi \\ \quad = \frac{1}{2\pi} \int_{-\pi}^{\pi} AF(\psi) e^{j(2m-1/2)\psi} d\psi & 1 \leq m \leq M \end{cases} \quad (7-14b)$$

Simplifications in the forms of (7-13a)–(7-13b) and (7-14a)–(7-14c) can be obtained when the excitations are symmetrical about the physical center of the array.

Example 7.3

Determine the excitation coefficients and the resultant pattern for a broadside discrete element array whose array factor closely approximates the desired symmetrical sectoral pattern of Example 7.2. Use 11 elements with a spacing of $d = \lambda/2$ between them. Repeat the design for 21 elements.

SOLUTION

Since the array is broadside, the progressive phase shift between the elements as required by (6-18a) is zero ($\beta = 0$). Since the pattern is nonzero only for $\pi/4 \leq \theta \leq 3\pi/4$, the corresponding values of ψ are obtained from (7-13c) or $\pi/\sqrt{2} \geq \psi \geq -\pi/\sqrt{2}$. The excitation coefficients are obtained from (7-14a) or

$$a_m = \frac{1}{2\pi} \int_{-\pi/\sqrt{2}}^{\pi/\sqrt{2}} e^{-jm\psi} d\psi = \frac{1}{\sqrt{2}} \left[\frac{\sin\left(\frac{m\pi}{\sqrt{2}}\right)}{\frac{m\pi}{\sqrt{2}}} \right]$$

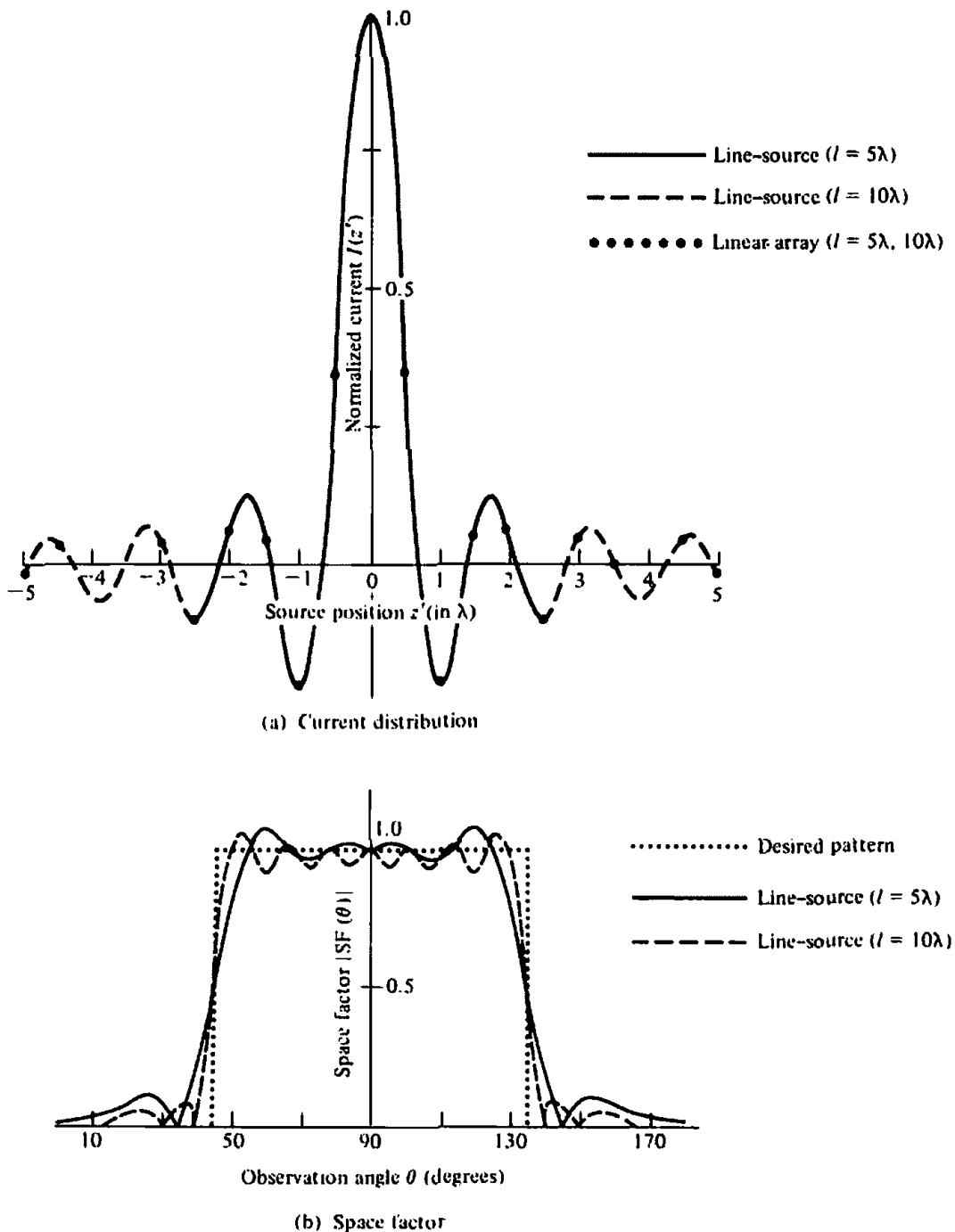


Figure 7.6 Normalized current distribution, desired pattern, and synthesized patterns using the Fourier transform method.

and they are symmetrical about the physical center of the array [$a_m(-z'_m) = a_m(z'_m)$]. The corresponding array factor is given by (7-13a).

The normalized excitation coefficients are

$$\begin{array}{lll}
 a_0 = 1.0000 & a_{\pm 4} = 0.0578 & a_{\pm 8} = -0.0496 \\
 a_{\pm 1} = 0.3582 & a_{\pm 5} = -0.0895 & a_{\pm 9} = 0.0455 \\
 a_{\pm 2} = -0.2170 & a_{\pm 6} = 0.0518 & a_{\pm 10} = -0.0100 \\
 a_{\pm 3} = 0.0558 & a_{\pm 7} = 0.0101 &
 \end{array}$$

They are displayed graphically by a dot (*) in Figure 7.6(a) where they are compared with the continuous current distribution of Example 7.2. It is apparent that at the

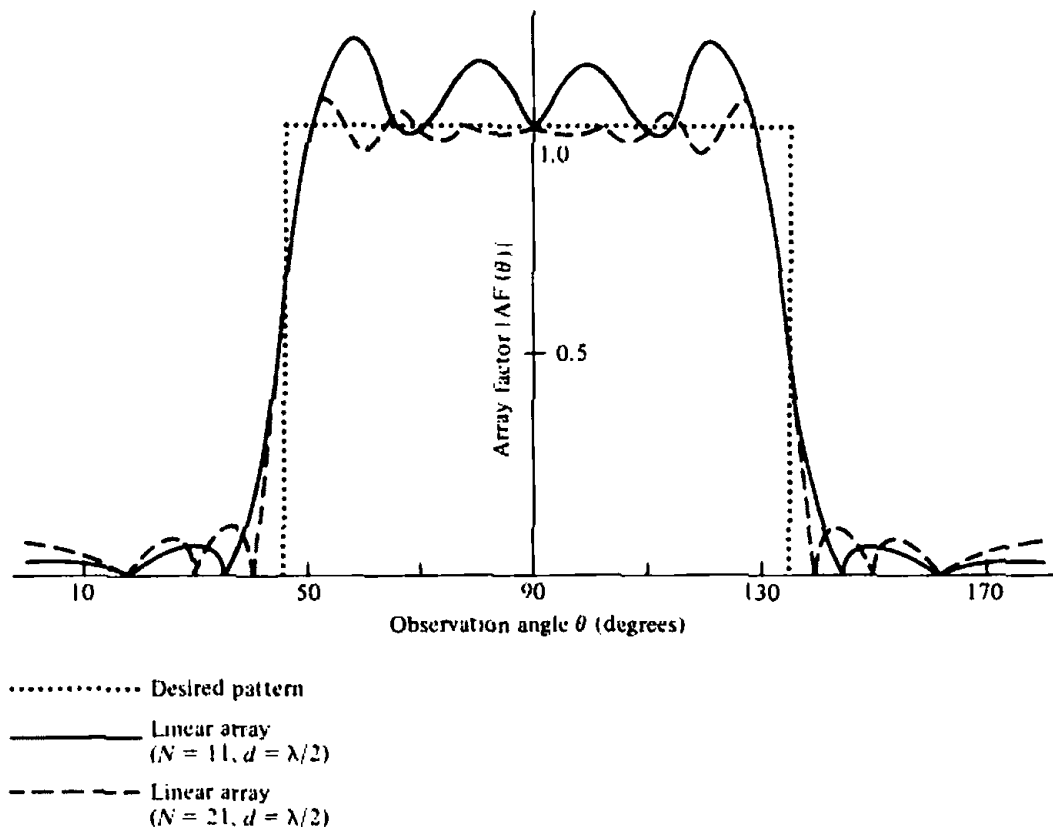


Figure 7.7 Desired array factor and synthesized normalized patterns for linear array of 11 and 21 elements using the Fourier transform method.

element positions, the line-source and linear array excitation values are identical. This is expected since the two antennas are of the same length (for $N = 11, d = \lambda/2 \Rightarrow l = 5\lambda$ and for $N = 21, d = \lambda/2 \Rightarrow l = 10\lambda$).

The corresponding normalized array factors are displayed in Figure 7.7. As it should be expected, the larger array ($N = 21, d = \lambda/2$) provides a better reconstruction of the desired pattern. The side lobe levels, relative to the value of the pattern at $\theta = 90^\circ$, are 0.061 (-24.29 dB) for $N = 11$ and 0.108 (-19.33 dB) for $N = 21$.

Discrete element linear arrays only approximate continuous line-sources. Therefore, their patterns shown in Figure 7.7 do not approximate as well the desired pattern as the corresponding patterns of the line-source distributions shown in Figure 7.6(b).

Whenever the desired pattern contains discontinuities or its values in a given region change very rapidly, the reconstruction pattern will exhibit oscillatory overshoots which are referred to as *Gibbs' phenomena*. Since the desired sectoral patterns of Examples 7.2 and 7.3 are discontinuous at $\theta = \pi/4$ and $3\pi/4$, the reconstructed patterns displayed in Figures 7.6(b) and 7.7 exhibit these oscillatory overshoots.

7.5 WOODWARD-LAWSON METHOD

A very popular antenna pattern synthesis method used for beam shaping was introduced by Woodward and Lawson [3], [4], [10]. The synthesis is accomplished by sampling the desired pattern at various discrete locations. Associated with each pattern sample is a harmonic current of uniform amplitude distribution and uniform progres-

sive phase, whose corresponding field is referred to as a *composing function*. For a line-source, each composing function is of an $b_m \sin(\psi_m)/\psi_m$ form whereas for a linear array it takes an $b_m \sin(N\phi_m)/N \sin(\phi_m)$ form. The excitation coefficient b_m of each harmonic current is such that its field strength is equal to the amplitude of the desired pattern at its corresponding sampled point. The total excitation of the source is comprised of a finite summation of space harmonics. The corresponding synthesized pattern is represented by a finite summation of composing functions with each term representing the field of a current harmonic with uniform amplitude distribution and uniform progressive phase.

The formation of the overall pattern using the Woodward-Lawson method is accomplished as follows. The first composing function produces a pattern whose main beam placement is determined by the value of its uniform progressive phase while its intermost side lobe level is about -13.5 dB; the level of the remaining side lobes monotonically decreases. The second composing function has also a similar pattern except that its uniform progressive phase is adjusted so that its main lobe maximum coincides with the intermost null of the first composing function. This results in the filling-in of the intermost null of the pattern of the first composing function; the amount of filling-in is controlled by the amplitude excitation of the second composing function. Similarly, the uniform progressive phase of the third composing function is adjusted so that the maximum of its main lobe occurs at the second intermost null of the first composing function; it also results in filling-in of the second intermost null of the first composing function. This process continues with the remaining finite number of composing functions.

The Woodward-Lawson method is simple, elegant and provides insight into the process of pattern synthesis. However, because the pattern of each composing function perturbs the entire pattern to be synthesized, it lacks local control over the side lobe level in the unshaped region of the entire pattern. In 1988 and 1989 a spirited and welcomed dialogue developed concerning the Woodward-Lawson method [11]–[14]. The dialogue centered whether the Woodward-Lawson method should be taught and even appear in textbooks, and whether it should be replaced by an alternate method [15] which overcomes some of the shortcomings of the Woodward-Lawson method. The alternate method of [15] is more of a numerical and iterative extension of Schelkunoff's polynomial method which may be of greater practical value because it provides superior beamshape and pattern control. One of the distinctions of the two methods is that the Woodward-Lawson method deals with the synthesis of *field patterns* while that of [15] deals with the synthesis of *power patterns*.

The analytical formulation of this method is similar to the Shannon sampling theorem used in communications which states that "if a function $g(t)$ is band-limited, with its highest frequency being f_h , the function $g(t)$ can be reconstructed using samples taken at a frequency f_s . To faithfully reproduce the original function $g(t)$, the sampling frequency f_s should be at least twice the highest frequency f_h ($f_s = 2f_h$) or the function should be sampled at points separated by no more than $\Delta t = 1/f_s = 1/(2f_h) = T_h/2$ where T_h is the period of the highest frequency f_h ." In a similar manner, the radiation pattern of an antenna can be synthesized by sampling functions whose samples are separated by λ/l rad, where l is the length of the source [9], [10].

7.5.1 Line-Source

Let the current distribution of a continuous source be represented, within $-l/2 \leq z' \leq l/2$, by a finite summation of normalized sources each of constant amplitude and linear phase of the form

$$i_m(z') = \frac{b_m}{l} e^{-jkz' \cos \theta_m} \quad -l/2 \leq z' \leq l/2 \quad (7-15)$$

As it will be shown later, θ_m represents the angles where the desired pattern is sampled. The total current $I(z')$ is given by a finite summation of $2M$ (even samples) or $2M + 1$ (odd samples) current sources each of the form of (7-15). Thus

$$I(z') = \frac{1}{l} \sum_{m=-M}^M b_m e^{-jkz' \cos \theta_m} \quad (7-16)$$

where

$$m = 0, \pm 1, \pm 2, \dots, \pm M \text{ (for } 2M + 1 \text{ odd number of samples)} \quad (7-16a)$$

For simplicity always use odd number of samples.

Associated with each current source of (7-15) is a corresponding field pattern of the form given by (7-9) or

$$s_m(\theta) = b_m \left\{ \frac{\sin \left[\frac{kl}{2} (\cos \theta - \cos \theta_m) \right]}{\frac{kl}{2} (\cos \theta - \cos \theta_m)} \right\} \quad (7-17)$$

whose maximum occurs when $\theta = \theta_m$. The total pattern is obtained by summing $2M + 1$ (odd samples) terms each of the form given by (7-17). Thus

$$SF(\theta) = \sum_{m=-M}^M b_m \left\{ \frac{\sin \left[\frac{kl}{2} (\cos \theta - \cos \theta_m) \right]}{\frac{kl}{2} (\cos \theta - \cos \theta_m)} \right\} \quad (7-18)$$

The maximum of each individual term in (7-18) occurs when $\theta = \theta_m$, and it is equal to $SF(\theta = \theta_m)$. In addition, when one term in (7-18) attains its maximum value at its sample at $\theta = \theta_m$, all other terms of (7-18) which are associated with the other samples are zero at $\theta = \theta_m$. In other words, all sampling terms (composing functions) of (7-18) are zero at all sampling points other than at their own. Thus at each sampling point the total field is equal to that of the sample. This is one of the most appealing properties of this method. If the desired space factor is sampled at $\theta = \theta_m$, the excitation coefficients b_m can be made equal to its value at the sample points θ_m . Thus

$$b_m = SF(\theta = \theta_m)_d \quad (7-19)$$

The reconstructed pattern is then given by (7-18), and it approximates closely the desired pattern.

In order for the synthesized pattern to satisfy the periodicity requirements of 2π for real values of θ (visible region) and to faithfully reconstruct the desired pattern, each sample should be separated by

$$kz' \Delta|_{|z'|=l} = 2\pi \Rightarrow \Delta = \frac{\lambda}{l} \quad (7-19a)$$

The location of each sample is given by

$$\cos\theta_m = m\Delta = m \left(\frac{\lambda}{l} \right), \quad m = 0, \pm 1, \pm 2, \dots \quad \text{for odd samples} \quad (7-19b)$$

$$\cos\theta_m = \begin{cases} \frac{(2m-1)}{2} \Delta = \frac{(2m-1)}{2} \left(\frac{\lambda}{l} \right), \\ \quad \quad \quad m = +1, +2, \dots \quad \text{for even samples} \\ \frac{(2m+1)}{2} \Delta = \frac{(2m+1)}{2} \left(\frac{\lambda}{l} \right), \\ \quad \quad \quad m = -1, -2, \dots \quad \text{for even samples} \end{cases} \quad (7-19c)$$

Therefore, M should be the closest integer to $M = l/\lambda$.

As long as the location of each sample is determined by (7-19b), the pattern value at the sample points is determined solely by that of one sample and it is not correlated to the field of the other samples.

Example 7.4

Repeat the design of Example 7.2 for $l = 5\lambda$ using odd samples and the Woodward-Lawson line-source synthesis method.

SOLUTION

Since $l = 5\lambda$, $M = 5$ and the sampling separation is 0.2. The total number of sampling points is 11. The angles where the sampling is performed are given, according to (7-19b), by

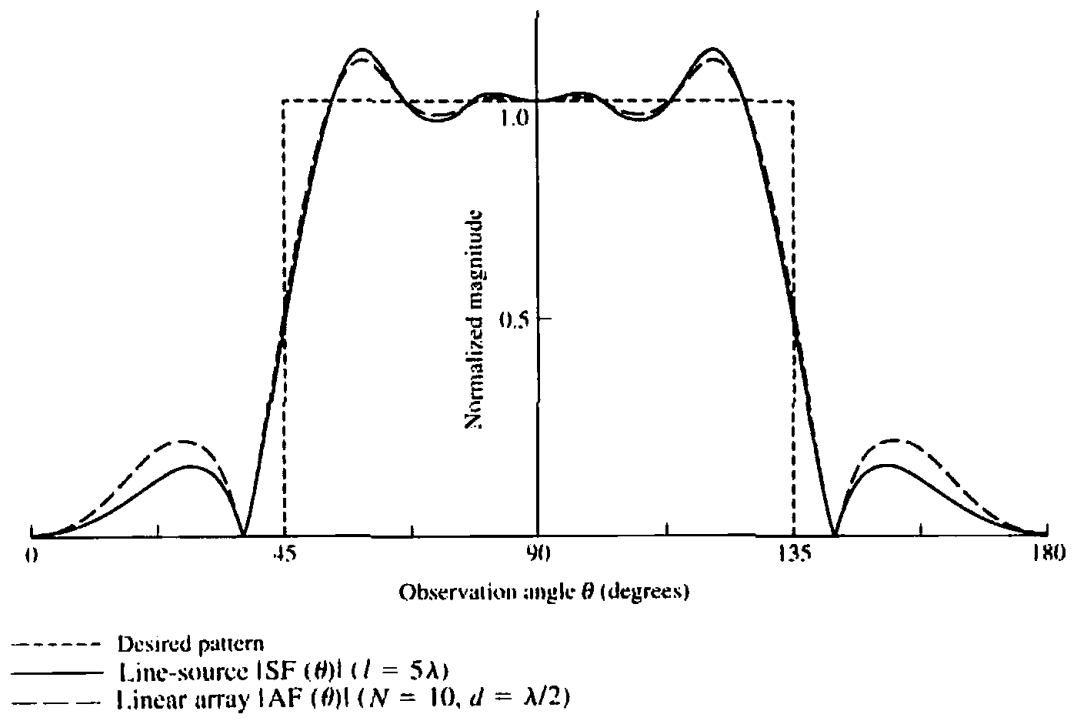
$$\theta_m = \cos^{-1} \left(m \frac{\lambda}{l} \right) = \cos^{-1}(0.2m), \quad m = 0, \pm 1, \dots, \pm 5$$

The angles and the excitation coefficients at the sample points are listed below.

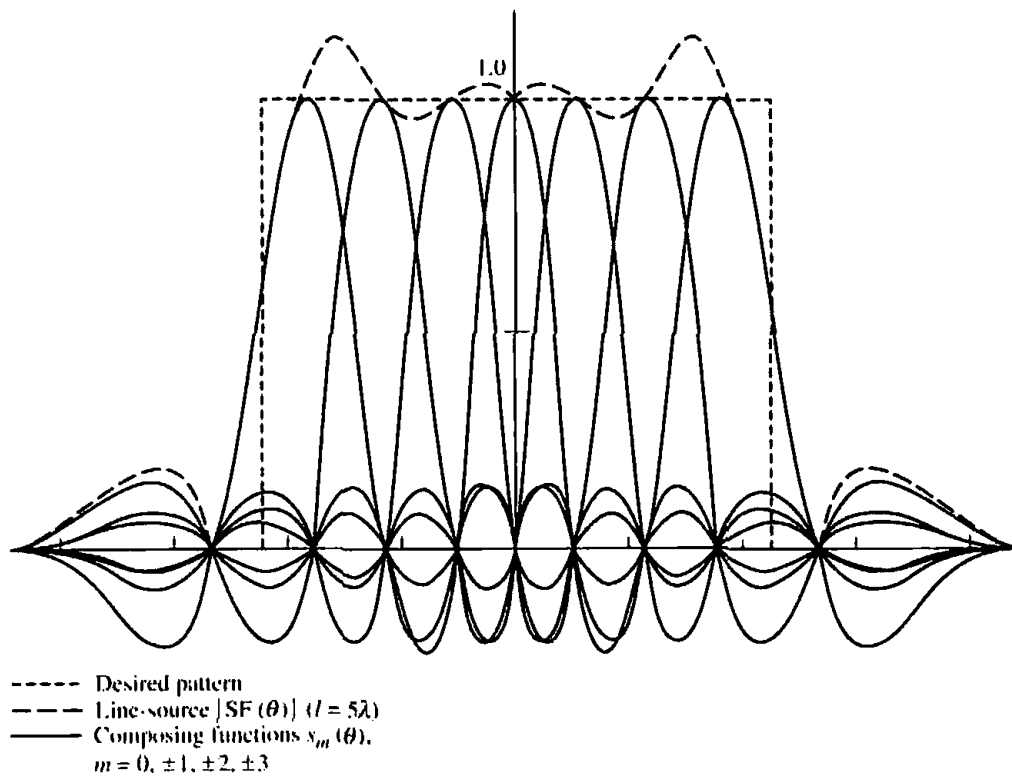
m	θ_m	$b_m = \text{SF}(\theta_m)_d$	m	θ_m	$b_m = \text{SF}(\theta_m)_d$
0	90°	1	-1	101.54°	1
1	78.46°	1	-2	113.58°	1
2	66.42°	1	-3	126.87°	1
3	53.13°	1	-4	143.13°	0
4	36.87°	0	-5	180°	0
5	0°	0			

The computed pattern is shown in Figure 7.8(a) where it is compared with the desired pattern. A good reconstruction is indicated. The side lobe level, relative to the value of the pattern at $\theta = 90^\circ$, is 0.160 (-15.92 dB).

To demonstrate the synthesis of the pattern using the sampling concept, we have plotted in Figure 7.8(b) all seven nonzero composing functions $s_m(\theta)$ used for the reconstruction of the $l = 5\lambda$ line-source pattern of Figure 7.8(a). Each nonzero $s_m(\theta)$ composing function was computed using (7-17) for $m = 0, \pm 1, \pm 2, \pm 3$. It is evident that at each sampling point all the composing functions are zero, except the one that represents that sample. Thus the value of the desired pattern at each sampling point is determined solely by the maximum value of a single composing function. The angles where the composing functions attain their maximum values are listed in the previous table.



(a) Normalized amplitude patterns



(b) Composing functions for line-source ($l = 5\lambda$)

Figure 7.8 Desired and synthesized patterns, and composing functions for Woodward-Lawson designs.

7.5.2 Linear Array

The Woodward-Lawson method can also be implemented to synthesize discrete linear arrays. The technique is similar to the Woodward-Lawson method for line sources except that the pattern of each sample, as given by (7-17), is replaced by the array factor of a uniform array as given by (6-10c). The pattern of each sample can be written as

$$f_m(\theta) = b_m \frac{\sin \left[\frac{N}{2} kd(\cos \theta - \cos \theta_m) \right]}{N \sin \left[\frac{1}{2} kd(\cos \theta - \cos \theta_m) \right]} \quad (7-20)$$

$\ell = Nd$ assumes the array is equal to the length of the line source (*the length ℓ of the line includes a distance $d/2$ beyond each end element*). The total array factor can be written as a superposition of $2M + 1$ sampling terms (as was done for the line source) each of the form of (7-20). Thus

$$AF(\theta) = \sum_{m=-M}^M b_m \frac{\sin \left[\frac{N}{2} kd(\cos \theta - \cos \theta_m) \right]}{N \sin \left[\frac{1}{2} kd(\cos \theta - \cos \theta_m) \right]} \quad (7-21)$$

As for the line sources, the excitation coefficients of the array elements at the sample points are equal to the value of the desired array factor at the sample points. That is,

$$b_m = AF(\theta = \theta_m) \quad (7-22)$$

The sample points are taken at

$$\cos \theta_m = m\Delta = m \left(\frac{\lambda}{l} \right), \quad m = 0, \pm 1, \pm 2, \dots \quad \text{for odd samples} \quad (7-23a)$$

$$\cos \theta_m = \begin{cases} \frac{(2m-1)}{2} \Delta = \frac{(2m-1)}{2} \left(\frac{\lambda}{Nd} \right), \\ \quad m = +1, +2, \dots & \text{for even samples} \\ \frac{(2m+1)}{2} \Delta = \frac{(2m+1)}{2} \left(\frac{\lambda}{Nd} \right), \\ \quad m = -1, -2, \dots & \text{for even samples} \end{cases} \quad (7-23b)$$

The normalized excitation coefficient of each array element, required to give the desired pattern, is given by

$$a_n(z') = \frac{1}{N_m} \sum_{m=-M}^M b_m e^{-jkz'_n \cos \theta_m} \quad (7-24)$$

where z'_n indicates the position of the n th element (element in question) symmetrically placed about the geometrical center of the array.

Example 7.5

Repeat the design of Example 7.4 for a linear array of 10 elements using the Woodward-Lawson method with odd samples and an element spacing of $d = \lambda/2$.

SOLUTION

According to (7-19), (7-19b), (7-22) and (7-23a), the excitation coefficients of the array at the sampling points are the same as those of the line source. Using the values of b_m as listed in Example 7.4, the computed array factor pattern using (7-21) is shown in Figure 7.8(a). A good synthesis of the desired pattern is displayed. The side lobe level, relative to the pattern value at $\theta = 90^\circ$, is 0.221 (–13.1 dB). The agreement between the line-source and the linear array Woodward-Lawson designs are also good.

The normalized pattern of the symmetrical discrete array can also be generated using the array factor of (6-61a) or (6-61b), where the normalized excitation coefficients a_n 's of the array elements are obtained using (7-24). For this example, the excitation coefficients of the 10-element array, along with their symmetrical position, are listed below. To achieve the normalized amplitude pattern of unity at $\theta = 90^\circ$ in Figure 7.8(a), the array factor of (6-61a) must be multiplied by $1/\sum a_n = 1/0.5 = 2.0$.

Element Number n	Element Position z'_n	Excitation Coefficient a_n
± 1	$\pm 0.25\lambda$	0.5695717
± 2	$\pm 0.75\lambda$	–0.0344577
± 3	$\pm 1.25\lambda$	–0.0999999
± 4	$\pm 1.75\lambda$	0.1108508
± 5	$\pm 2.25\lambda$	–0.0459650

In general, the Fourier transform synthesis method yields reconstructed patterns whose mean-square error (or deviation) from the desired pattern is a minimum. However, the Woodward-Lawson synthesis method reconstructs patterns whose values at the sampled points are identical to the ones of the desired pattern; it does not have any control of the pattern between the sample points, and it does not yield a pattern with least mean-square deviation.

Ruze [9] points out that the least-mean-square error design is not necessarily the best. The particular application will dictate the preference between the two. However, the Fourier transform method is best suited for reconstruction of desired patterns which are analytically simple and which allow the integrations to be performed in closed form. Today, with the advent of high-speed computers, this is not a major restriction since integration can be performed (with high efficiency) numerically. In contrast, the Woodward-Lawson method is more flexible, and it can be used to synthesize any desired pattern. In fact, it can even be used to reconstruct patterns which, because of their complicated nature, cannot be expressed analytically. Measured patterns, either of analog or digital form, can also be synthesized using the Woodward-Lawson method.

7.6 TAYLOR LINE-SOURCE (TSCHEBYSCHEFF ERROR)

In Chapter 6 we discussed the classic Dolph-Tschebyscheff array design which yields, for a given side lobe level, the smallest possible first null beamwidth (or the smallest possible side lobe level for a given first null beamwidth). Another classic design that

is closely related to it, but is more applicable for continuous distributions, is that by Taylor [5] (this method is different from that by Taylor [6] which will be discussed in the next section).

The Taylor design [5] yields a pattern that is an optimum compromise between beamwidth and side lobe level. In an ideal design, the minor lobes are maintained at an equal and specific level. Since the minor lobes are of equal ripple and extend to infinity, this implies an infinite power. More realistically, however, the technique as introduced by Taylor leads to a pattern whose first few minor lobes (closest to the main lobe) are maintained at an equal and specified level; the remaining lobes decay monotonically. Practically, even the level of the closest minor lobes exhibits a slight monotonic decay. This decay is a function of the space u over which these minor lobes are required to be maintained at an equal level. As this space increases, the rate of decay of the closest minor lobes decreases. For a very large space of u (over which the closest minor lobes are required to have an equal ripple), the rate of decay is negligible. It should be pointed out, however, that the other method by Taylor [6] (of Section 7.7) yields minor lobes, all of which decay monotonically.

The details of the analytical formulation are somewhat complex (for the average reader) and lengthy, and they will not be included here. The interested reader is referred to the literature [5], [16]. Instead, a succinct outline of the salient points of the method and of the design procedure will be included. The design is for far-field patterns, and it is based on the formulation of (7-1).

Ideally the normalized space factor that yields a pattern with equal-ripple minor lobes is given by

$$SF(\theta) = \frac{\cosh [\sqrt{(\pi A)^2 - u^2}]}{\cosh(\pi A)} \tag{7-25}$$

$$u = \pi \frac{l}{\lambda} \cos \theta \tag{7-25a}$$

whose maximum value occurs when $u = 0$. The constant A is related to the maximum desired side lobe level R_0 by

$$\cosh(\pi A) = R_0 \text{ (voltage ratio)} \tag{7-26}$$

The space factor of (7-25) can be derived from the Dolph-Tschebyscheff array formulation of Section 6.8.3, if the number of elements of the array are allowed to become infinite.

Since (7-25) is ideal and cannot be realized physically, Taylor [5] suggested that it be approximated (within a certain error) by a space factor comprised of a product of factors whose roots are the zeros of the pattern. Because of its approximation to the ideal Tschebyscheff design, it is also referred to as *Tschebyscheff error*. The Taylor space factor is given by

$$SF(u, A, \bar{n}) = \frac{\sin(u)}{u} \frac{\prod_{n=1}^{\bar{n}-1} \left[1 - \left(\frac{u}{u_n} \right)^2 \right]}{\prod_{n=1}^{\bar{n}-1} \left[1 - \left(\frac{u}{n\pi} \right)^2 \right]} \tag{7-27}$$

$$u = \pi v = \pi \frac{l}{\lambda} \cos \theta \quad (7-27a)$$

$$u_n = \pi v_n = \pi \frac{l}{\lambda} \cos \theta_n \quad (7-27b)$$

where θ_n represents the locations of the nulls. The parameter \bar{n} is a constant chosen by the designer so that the minor lobes for $|v| = |u/\pi| \leq \bar{n}$ are maintained at a nearly constant voltage level of $1/R_0$; for $|v| = |u/\pi| > \bar{n}$ the envelope, through the maxima of the remaining minor lobes, decays at a rate of $1/v = \pi/u$. In addition, the nulls of the pattern for $|v| \geq \bar{n}$ occur at integer values of v .

In general, there are $\bar{n} - 1$ inner nulls for $|v| < \bar{n}$ and an infinite number of outer nulls for $|v| \geq \bar{n}$. To provide a smooth transition between the inner and the outer nulls (at the expense of slight beam broadening), Taylor introduced a parameter σ . It is usually referred to as the *scaling factor*, and it spaces the inner nulls so that they blend smoothly with the outer ones. In addition, it is the factor by which the beamwidth of the Taylor design is greater than that of the Dolph-Tschebyscheff, and it is given by

$$\sigma = \frac{\bar{n}}{\sqrt{A^2 + (\bar{n} - \frac{1}{2})^2}} \quad (7-28)$$

The location of the nulls are obtained using

$$u_n = \pi v_n = \pi \frac{l}{\lambda} \cos \theta_n = \begin{cases} \pm \pi \sigma \sqrt{A^2 + (n - \frac{1}{2})^2} & 1 \leq n < \bar{n} \\ \pm n \pi & \bar{n} \leq n \leq \infty \end{cases} \quad (7-29)$$

The normalized line-source distribution, which yields the desired pattern, is given by

$$I(z') = \frac{\lambda}{l} \left[1 + 2 \sum_{p=1}^{\bar{n}-1} \text{SF}(p, A, \bar{n}) \cos \left(2\pi p \frac{z'}{l} \right) \right] \quad (7-30)$$

The coefficients $\text{SF}(p, A, \bar{n})$ represent samples of the Taylor pattern, and they can be obtained from (7-27) with $u = \pi p$. They can also be found using

$$\text{SF}(p, A, \bar{n}) = \begin{cases} \frac{[(\bar{n} - 1)!]^2}{(\bar{n} - 1 + p)!(\bar{n} - 1 - p)!} \prod_{m=1}^{\bar{n}-1} \left[1 - \left(\frac{\pi p}{u_m} \right)^2 \right] & |p| < \bar{n} \\ 0 & |p| \geq \bar{n} \end{cases} \quad (7-30a)$$

with $\text{SF}(-p, A, \bar{n}) = \text{SF}(p, A, \bar{n})$.

The half-power beamwidth is given approximately by [8]

$$\Theta_0 \approx 2 \sin^{-1} \left\{ \frac{\lambda \sigma}{\pi l} \left[(\cosh^{-1} R_0)^2 - \left(\cosh^{-1} \frac{R_0}{\sqrt{2}} \right)^2 \right]^{1/2} \right\} \quad (7-31)$$

7.6.1 Design Procedure

To initiate a Taylor design, you must

1. specify the normalized maximum tolerable side lobe level $1/R_0$ of the pattern.

2. choose a positive integer value for \bar{n} such that for $|v| = |(l/\lambda) \cos \theta| \leq \bar{n}$ the normalized level of the minor lobes is nearly constant at $1/R_0$. For $|v| > \bar{n}$, the minor lobes decrease monotonically. In addition, for $|v| < \bar{n}$ there exist $(\bar{n} - 1)$ nulls. The position of all the nulls is found using (7-29). Small values of \bar{n} yield source distributions which are maximum at the center and monotonically decrease toward the edges. In contrast, large values of \bar{n} result in sources which are peaked simultaneously at the center and at the edges, and they yield sharper main beams. Therefore, very small and very large values of \bar{n} should be avoided. Typically, the value of \bar{n} should be at least 3 and at least 6 for designs with side lobes of -25 and -40 dB, respectively.

To complete the design, you do the following:

1. Determine A using (7-26), σ using (7-28), and the nulls using (7-29).
2. Compute the space factor using (7-27), the source distribution using (7-30) and (7-30a), and the half-power beamwidth using (7-31).

Example 7.6

Design a -20 dB Taylor distribution line-source with $\bar{n} = 5$. Plot the pattern and the current distribution for $l = 7\lambda$ ($-7 \leq v = u/\pi \leq 7$).

SOLUTION

For a -20 dB side lobe level

$$R_0 \text{ (voltage ratio)} = 10$$

Using (7-26)

$$A = \frac{1}{\pi} \cosh^{-1}(10) = 0.95277$$

and by (7-28)

$$\sigma = \frac{5}{\sqrt{(0.95277)^2 + (5 - 0.5)^2}} = 1.0871$$

The nulls are given by (7-29) or

$$v_n = u_n/\pi = \pm 1.17, \pm 1.932, \pm 2.91, \pm 3.943, \pm 5.00, \pm 6.00, \pm 7.00, \dots$$

The corresponding null angles for $l = 7\lambda$ are

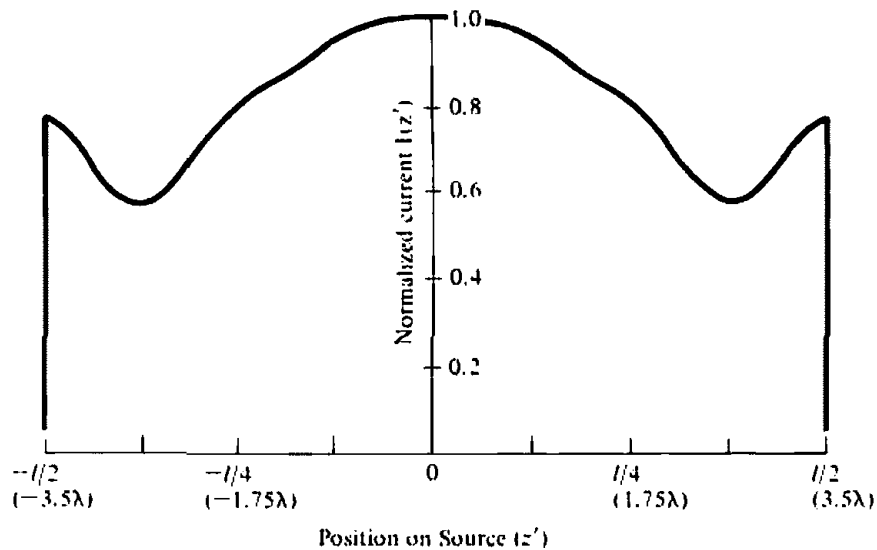
$$\theta_n = 80.38^\circ (99.62^\circ), 73.98^\circ (106.02^\circ), 65.45^\circ (114.55^\circ), \\ 55.71^\circ (124.29^\circ), 44.41^\circ (135.59^\circ), \text{ and } 31.00^\circ (149.00^\circ)$$

The half-power beamwidth for $l = 7\lambda$ is found using (7-31), or

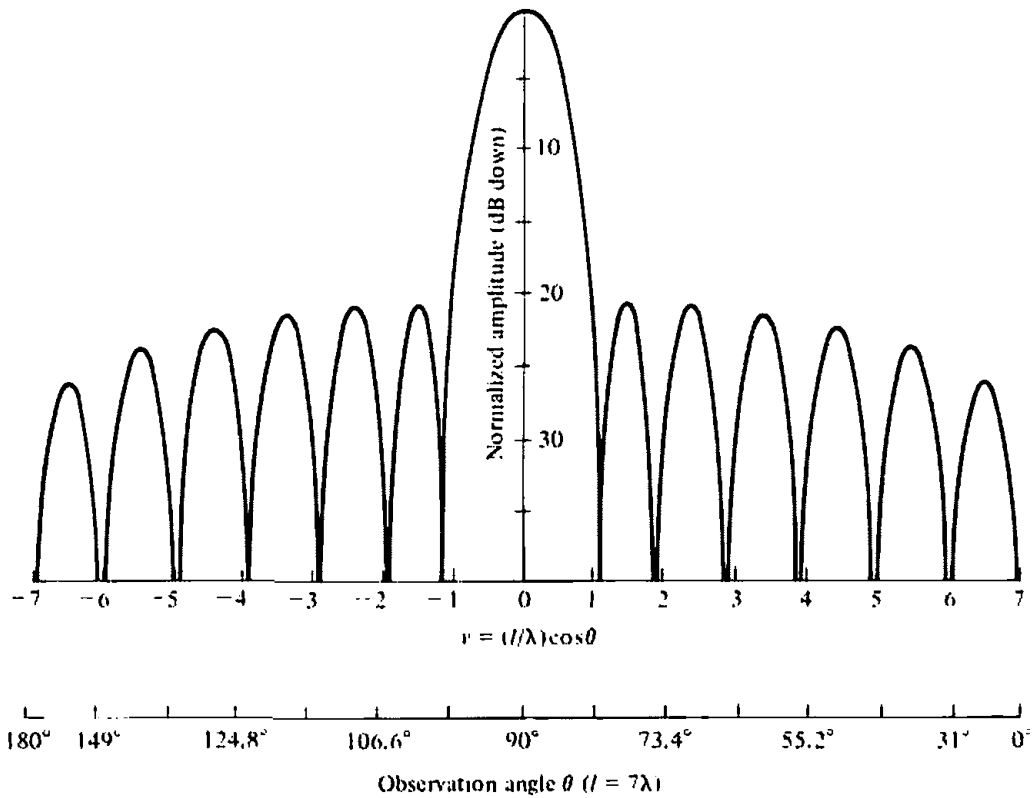
$$\Theta_0 \approx 7.95^\circ$$

The source distribution, as computed using (7-30) and (7-30a), is displayed in Figure 7.9(a). The corresponding radiation pattern for $-7 \leq v = u/\pi \leq 7$ ($0^\circ \leq \theta \leq 180^\circ$ for $l = 7\lambda$) is shown in Figure 7.9(b).

All the computed parameters compare well with results reported in [5] and [16].



(a) Current distribution



(b) Space factor

Figure 7.9 Normalized current distribution and far-field space factor pattern for a -20 dB side lobe and $\bar{n} = 5$ Taylor (Tschebyscheff error) line-source of $l = 7\lambda$.

7.7 TAYLOR LINE-SOURCE (ONE-PARAMETER)

The Dolph-Tschebyscheff array design of Section 6.8.3 yields minor lobes of equal intensity while the Taylor (Tschebyscheff error) produces a pattern whose inner minor lobes are maintained at a constant level and the remaining ones decrease monotonically. For some applications, such as radar and low-noise systems, it is desirable to

sacrifice some beamwidth and low inner minor lobes to have all the minor lobes decay as the angle increases on either side of the main beam. In radar applications this is preferable because interfering or spurious signals would be reduced further when they try to enter through the decaying minor lobes. Thus any significant contributions from interfering signals would be through the pattern in the vicinity of the major lobe. Since in practice it is easier to maintain pattern symmetry around the main lobe, it is also possible to recognize that such signals are false targets. In low-noise applications, it is also desirable to have minor lobes that decay away from the main beam in order to diminish the radiation accepted through them from the relatively ‘hot’ ground.

A continuous line-source distribution that yields decaying minor lobes and, in addition, controls the amplitude of the side lobe is that introduced by Taylor [6] in an unpublished classic memorandum. It is referred to as the *Taylor (one-parameter)* design and its source distribution is given by

$$I_n(z') = \begin{cases} J_0 \left[j \pi B \sqrt{1 - \left(\frac{2z'}{l} \right)^2} \right] & -l/2 \leq z' \leq +l/2 \\ 0 & \text{elsewhere} \end{cases} \quad (7-32)$$

where J_0 is the Bessel function of the first kind of order zero, l is the total length of the continuous source [see Figure 7.1(a)], and B is a constant to be determined from the specified side lobe level.

The space factor associated with (7-32) can be obtained by using (7-1). After some intricate mathematical manipulations, utilizing Gegenbauer’s finite integral and Gegenbauer polynomials [17], the space factor for a Taylor amplitude distribution line-source with uniform phase [$\phi_n(z') = \phi_0 = 0$] can be written as

$$SF(\theta) = \begin{cases} l \frac{\sinh[\sqrt{(\pi B)^2 - u^2}]}{\sqrt{(\pi B)^2 - u^2}}, & u^2 < (\pi B)^2 \\ l \frac{\sin[\sqrt{u^2 - (\pi B)^2}]}{\sqrt{u^2 - (\pi B)^2}}, & u^2 > (\pi B)^2 \end{cases} \quad (7-33)$$

where

$$u = \pi \frac{l}{\lambda} \cos \theta \quad (7-33a)$$

B = constant determined from side lobe level

l = line-source dimension

The derivation of (7-33) is assigned as an exercise to the reader (Problem 7.17). When $(\pi B)^2 > u^2$, (7-33) represents the region near the main lobe. The minor lobes are represented by $(\pi B)^2 < u^2$ in (7-33). Either form of (7-33) can be obtained from the other by knowing that (see Appendix VI)

$$\begin{aligned} \sin(jx) &= j \sinh(x) \\ \sinh(jx) &= j \sin(x) \end{aligned} \quad (7-34)$$

When $u = 0$ ($\theta = \pi/2$ and maximum radiation), the normalized pattern height is equal to

$$(\text{SF})_{\text{max}} = \frac{\sinh(\pi B)}{\pi B} = H_0 \quad (7-35)$$

For $u^2 \gg (\pi B)^2$, the normalized form of (7-33) reduces to

$$\text{SF}(\theta) = \frac{\sin[\sqrt{u^2 - (\pi B)^2}]}{\sqrt{u^2 - (\pi B)^2}} \approx \frac{\sin(u)}{u} \quad u \gg \pi B \quad (7-36)$$

and it is identical to the pattern of a uniform distribution. The maximum height H_1 of the side lobe of (7-36) is $H_1 = 0.217233$ (or 13.2 dB down from the maximum), and it occurs when (see Appendix I)

$$[u^2 - (\pi B)^2]^{1/2} \approx u = 4.494 \quad (7-37)$$

Using (7-35), the maximum voltage height of the side lobe (relative to the maximum H_0 of the major lobe) is equal to

$$\frac{H_1}{H_0} = \frac{1}{R_0} = \frac{0.217233}{\sinh(\pi B)/(\pi B)} \quad (7-38)$$

or

$$R_0 = \frac{1}{0.217233} \frac{\sinh(\pi B)}{\pi B} = 4.603 \frac{\sinh(\pi B)}{\pi B} \quad (7-38a)$$

Equation (7-38a) can be used to find the constant B when the intensity ratio R_0 of the major-to-the-side lobe is specified. Values of B for typical side lobe levels are

SIDE LOBE LEVEL (dB)	-10	-15	-20	-25	-30	-35	-40
B	0.4597	0.3558	0.7386	1.0229	1.2761	1.5136	1.7415

The disadvantage of designing an array with decaying minor lobes as compared to a design with equal minor lobe level (Dolph-Tschebyscheff), is that it yields about 12 to 15% greater half-power beamwidth. However such a loss in beamwidth is a small penalty to pay when the extreme minor lobes decrease as $1/u$.

To illustrate the principles, let us consider an example.

Example 7.7

Given a continuous line-source, whose total length is 4λ , design a Taylor distribution array whose side lobe is 30 dB down from the maximum of the major lobe.

- Find the constant B .
- Plot the pattern (in dB) of the continuous line-source distribution.

- (c) For a spacing of $\lambda/4$ between the elements, find the number of discrete isotropic elements needed to approximate the continuous source. Assume that the two extreme elements are placed at the edges of the continuous line source.
- (d) Find the normalized coefficients of the discrete array of part (c).
- (e) Write the array factor of the discrete array of parts (c) and (d).
- (f) Plot the array factor (in dB) of the discrete array of part (e).
- (g) For a corresponding Dolph-Tschebyscheff array, find the normalized coefficients of the discrete elements.
- (h) Compare the patterns of the Taylor continuous line-source distribution and discretized array, and the corresponding Dolph-Tschebyscheff discrete element array.

SOLUTION

For a -30 dB maximum side lobe, the voltage ratio of the major-to-the-side lobe level is equal to

$$30 = 20 \log_{10} (R_0) \Rightarrow R_0 = 31.62$$

- (a) The constant B is obtained using (7-38a) or

$$R_0 = 31.62 = 4.603 \frac{\sinh(\pi B)}{\pi B} \Rightarrow B = 1.2761$$

- (b) The normalized space factor pattern is obtained using (7-33), and it is shown plotted in Figure 7.10.
- (c) For $d = \lambda/4$ and with elements at the extremes, the number of elements is 17.
- (d) The coefficients are obtained using (7-32). Since we have an odd number of elements, their positioning and excitation coefficients are those shown in Figure 6.17(b). Thus the total excitation coefficient of the center element is

$$2a_1 = I_n(z')|_{z'=0} = J_0(j4.009) = 11.400 \Rightarrow a_1 = 5.70$$

The coefficients of the elements on either side of the center element are identical (because of symmetry), and they are obtained from

$$a_2 = I(z')|_{z'=\pm\lambda/4} = J_0(j3.977) = 11.106$$

The coefficients of the other elements are obtained in a similar manner, and they are given by

$$a_3 = 10.192$$

$$a_4 = 8.889$$

$$a_5 = 7.195$$

$$a_6 = 5.426$$

$$a_7 = 3.694$$

$$a_8 = 2.202$$

$$a_9 = 1.000$$

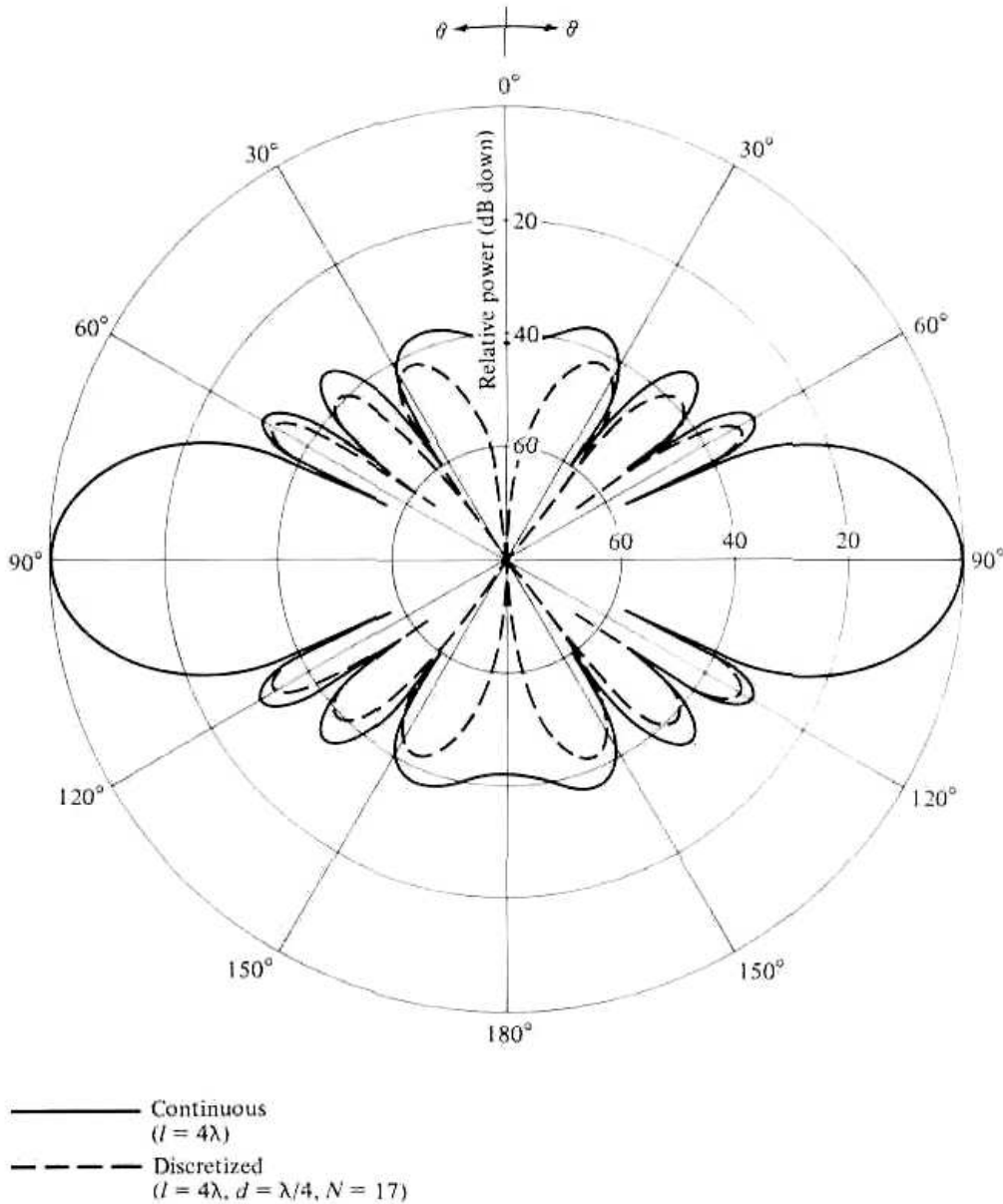


Figure 7.10 Far-field amplitude patterns of continuous and discretized Taylor (one-parameter) distributions.

- (e) The array factor is given by (6-61b) and (6-61c), or

$$\begin{aligned}
 (\text{AF})_{17} &= \sum_{n=1}^9 a_n \cos[2(n-1)u] \\
 u &= \pi \frac{d}{\lambda} \cos \theta = \frac{\pi}{4} \cos \theta
 \end{aligned}$$

where the coefficients (a_n 's) are those found in part (d).

- (f) The normalized pattern (in dB) of the discretized distribution (discrete element array) is shown in Figure 7.10.
- (g) The normalized coefficients of a 17-element Dolph-Tschebyscheff array, with -30 dB side lobes, are obtained using the method outlined in the Design Section of Section 6.8.3 and are given by

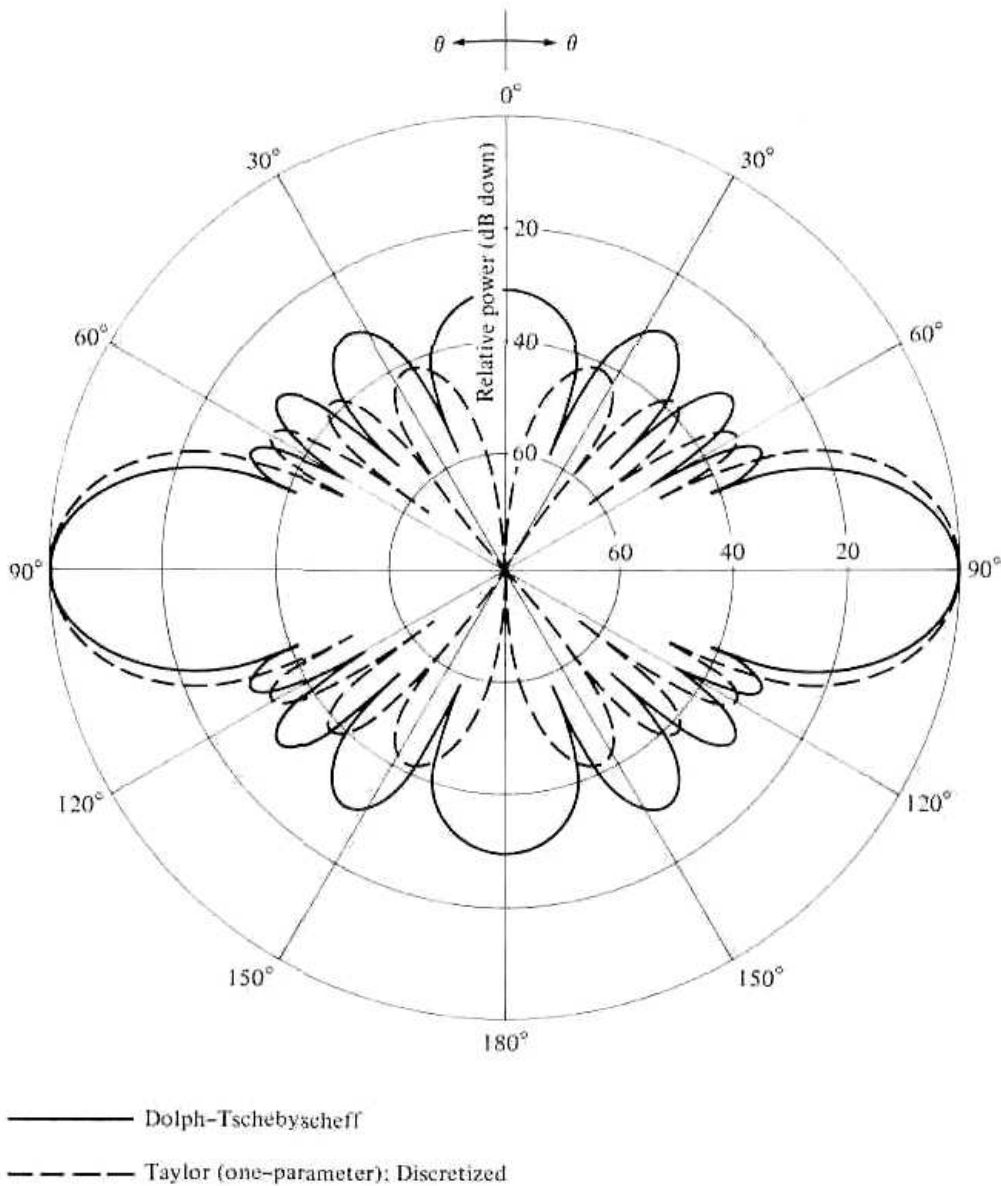


Figure 7.11 Far-field amplitude patterns of Taylor (discretized) and Dolph-Tschebyscheff distributions ($l = 4\lambda$, $d = \lambda/4$, $N = 17$).

UNNORMALIZED	NORMALIZED
$a_1 = 2.858$	$a_{1n} = 1.680$
$a_2 = 5.597$	$a_{2n} = 3.290$
$a_3 = 5.249$	$a_{3n} = 3.086$
$a_4 = 4.706$	$a_{4n} = 2.767$
$a_5 = 4.022$	$a_{5n} = 2.364$
$a_6 = 3.258$	$a_{6n} = 1.915$
$a_7 = 2.481$	$a_{7n} = 1.459$
$a_8 = 1.750$	$a_{8n} = 1.029$
$a_9 = 1.701$	$a_{9n} = 1.000$

As with the discretized Taylor distribution array, the coefficients are symmetrical, and the form of the array factor is that given in part (e).

(h) The normalized pattern (in dB) is plotted in Figure 7.11 where it is compared

with that of the discretized Taylor distribution. From the patterns in Figures 7.10 and 7.11, it can be concluded that

1. the main lobe of the continuous line-source Taylor design is well approximated by the discretized distribution with a $\lambda/4$ spacing between the elements. Even the minor lobes are well represented, and a better approximation can be obtained with more elements and smaller spacing between them.
2. the Taylor distribution array pattern has a wider main lobe than the corresponding Dolph-Tschebyscheff, but it displays decreasing minor lobes away from the main beam.

A larger spacing between the elements does not approximate the continuous distribution as accurately. The design of Taylor and Dolph-Tschebyscheff arrays for $l = 4\lambda$ and $d = \lambda/2$ ($N = 9$) is assigned as a problem at the end of the chapter (Problem 7.18).

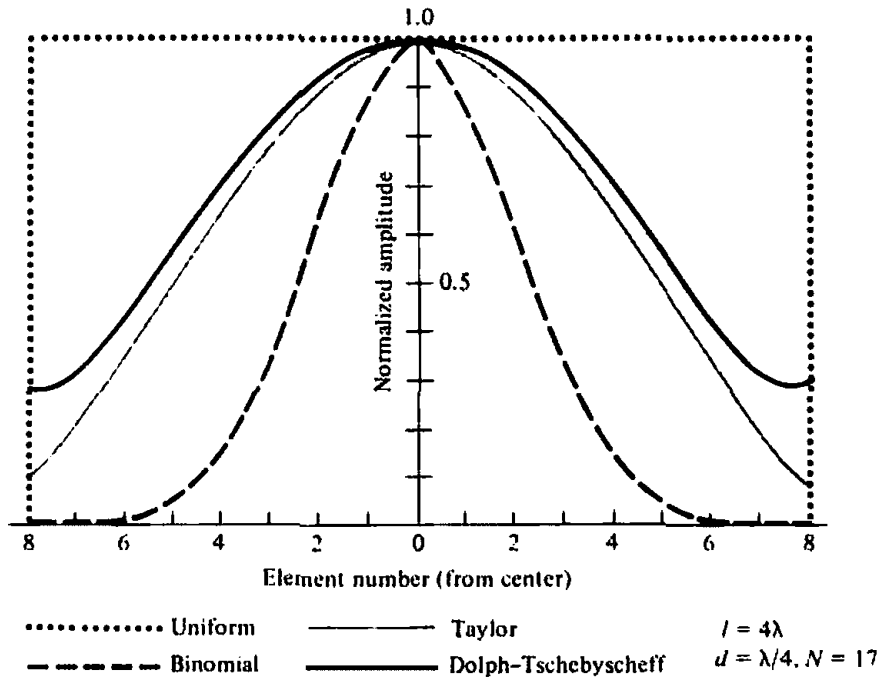
To qualitatively assess the performance between uniform, binomial, Dolph-Tschebyscheff, and Taylor (one-parameter) array designs, the amplitude distribution of each has been plotted in Figure 7.12(a). It is assumed that $l = 4\lambda$, $d = \lambda/4$, $N = 17$, and the maximum side lobe is 30 dB down. The coefficients are normalized with respect to the amplitude of the corresponding element at the center of that array.

The binomial design possesses the smoothest amplitude distribution (between 1 and 0) from the center to the edges (the amplitude toward the edges is vanishingly small). Because of this characteristic, the binomial array displays the smallest side lobes followed, in order, by the Taylor, Tschebyscheff, and the uniform arrays. In contrast, the uniform array possesses the smallest half-power beamwidth followed, in order, by the Tschebyscheff, Taylor, and binomial arrays. As a rule of thumb, the array with the smoothest amplitude distribution (from the center to the edges) has the smallest side lobes and the larger half-power beamwidths. The best design is a trade-off between side lobe level and beamwidth.

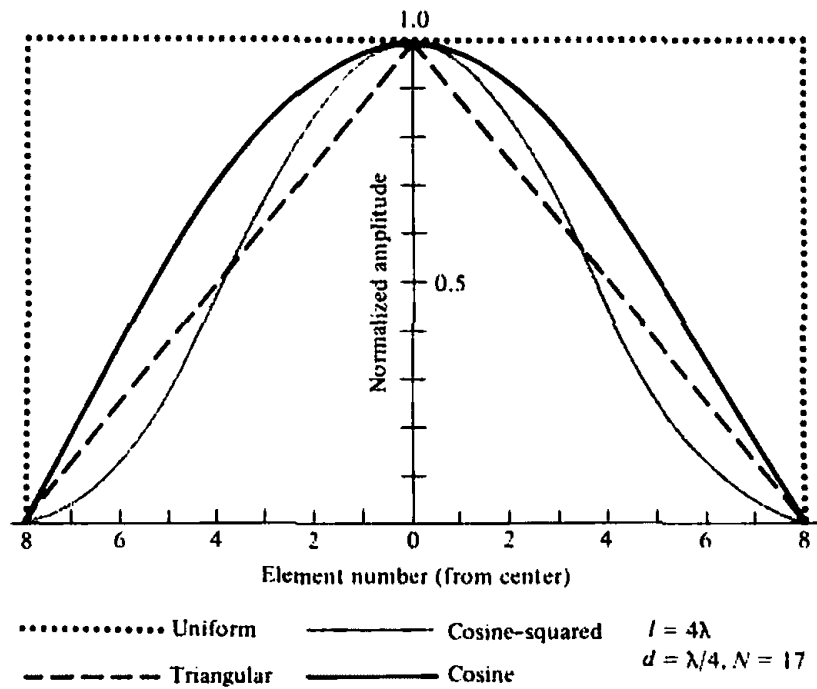
7.8 TRIANGULAR, COSINE, AND COSINE-SQUARED AMPLITUDE DISTRIBUTIONS

Some other very common and simple line-source amplitude distributions are those of the triangular, cosine, cosine-squared, cosine on-a-pedestal, cosine-squared on-a-pedestal, Gaussian, inverse taper, and edge. Instead of including many details, the pattern, half-power beamwidth, first-null beamwidth, magnitude of side lobes, and directivity for uniform, triangular, cosine, and cosine-squared amplitude distributions (with constant phase) are summarized in Table 7.1 [18], [19].

The normalized coefficients for a uniform, triangular, cosine, and cosine-squared arrays of $l = 4\lambda$, $d = \lambda/4$, $N = 17$ are shown plotted in Figure 7.12(b). The array with the smallest side lobes and the larger half-power beamwidth is the cosine-squared, because it possesses the smoothest distribution. It is followed, in order, by the triangular, cosine, and uniform distributions. This is verified by examining the characteristics in Table 7.1.



(a) Amplitude distribution of uniform, binomial, Taylor, and Dolph-Tschebyscheff discrete-element arrays



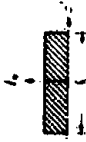



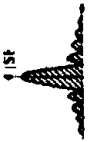



(b) Amplitude distribution of uniform, triangular, cosine, and cosine squared discrete-element arrays

Figure 7.12 Amplitude distribution of nonuniform amplitude linear arrays.

Cosine on-a-pedestal distribution is obtained by the superposition of the uniform and the cosine distributions. Thus it can be represented by

$$I_n(z') = \begin{cases} I_0 + I_2 \cos\left(\frac{\pi}{l} z'\right), & -l/2 \leq z' \leq l/2 \\ 0 & \text{elsewhere} \end{cases} \quad (7-39)$$

Table 7.1 RADIATION CHARACTERISTICS FOR LINE SOURCES AND LINEAR ARRAYS WITH UNIFORM, TRIANGULAR, COSINE, AND COSINE-SQUARED DISTRIBUTIONS

Distribution	Uniform	Triangular	Cosine	Cosine-Squared
Distribution I_n (analytical)	I_0	$I_1 \left(1 - \frac{2}{l} z' \right)$	$I_2 \cos \left(\frac{\pi}{l} z' \right)$	$I_3 \cos^2 \left(\frac{\pi}{l} z' \right)$
Distribution (graphical)				
Space factor (SF) $u = \left(\frac{\pi l}{\lambda} \right) \cos \theta$	$I_0 l \frac{\sin(u)}{u}$	$I_1 \frac{1}{2} \left[\frac{\sin \left(\frac{u}{2} \right)}{\frac{u}{2}} \right]^2$	$I_2 l \frac{\pi}{2} \frac{\cos(u)}{(\pi/2)^2 - u^2}$	$I_3 \frac{l}{2} \frac{\sin(u)}{u} \left[\frac{\pi^2}{\pi^2 - u^2} \right]$
Space factor SF				
Half-power beamwidth (degrees) $l \gg \lambda$	$\frac{50.6}{(l/\lambda)}$	$\frac{73.4}{(l/\lambda)}$	$\frac{68.8}{(l/\lambda)}$	$\frac{83.2}{(l/\lambda)}$
First null beamwidth (degrees) $l \gg \lambda$	$\frac{114.6}{(l/\lambda)}$	$\frac{229.2}{(l/\lambda)}$	$\frac{171.9}{(l/\lambda)}$	$\frac{229.2}{(l/\lambda)}$
First side lobe max. (to main max.) (dB)	-13.2	-26.4	-23.2	-31.5
Directivity factor (l large)	$2 \left(\frac{l}{\lambda} \right)$	$0.75 \left[2 \left(\frac{l}{\lambda} \right) \right]$	$0.810 \left[2 \left(\frac{l}{\lambda} \right) \right]$	$0.667 \left[2 \left(\frac{l}{\lambda} \right) \right]$

where I_0 and I_2 are constants. The space factor pattern of such a distribution is obtained by the addition of the patterns of the uniform and the cosine distributions found in Table 7.1. That is,

$$\text{SF}(\theta) = I_0 l \frac{\sin(u)}{u} + I_2 \frac{\pi l}{2} \frac{\cos u}{(\pi/2)^2 - u^2} \quad (7-40)$$

A similar procedure is used to represent and analyze a cosine-squared on-a-pedestal distribution.

7.9 LINE-SOURCE PHASE DISTRIBUTIONS

The amplitude distributions of the previous section were assumed to have uniform phase variations throughout the physical extent of the source. Practical radiators (such as reflectors, lenses, horns, etc.) have nonuniform phase fronts caused by one or more of the following:

1. displacement of the reflector feed from the focus
2. distortion of the reflector or lens surface
3. feeds whose wave fronts are not ideally cylindrical or spherical (as they are usually presumed to be)
4. physical geometry of the radiator

These are usually referred to *phase errors*, and they are more evident in radiators with tilted beams.

To simplify the analytical formulations, most of the phase fronts are represented with linear, quadratic, or cubic distributions. Each of the phase distributions can be associated with each of the amplitude distributions. In (7-1), the phase distribution of the source is represented by $\phi_n(z')$. For linear, quadratic, and cubic phase variations, $\phi_n(z')$ takes the form of

$$\text{linear:} \quad \phi_1(z') = \beta_1 \frac{2}{l} z', \quad -l/2 \leq z' \leq l/2 \quad (7-41a)$$

$$\text{quadratic:} \quad \phi_2(z') = \beta_2 \left(\frac{2}{l}\right)^2 z'^2, \quad -l/2 \leq z' \leq l/2 \quad (7-41b)$$

$$\text{cubic:} \quad \phi_3(z') = \beta_3 \left(\frac{2}{l}\right)^3 z'^3, \quad -l/2 \leq z' \leq l/2 \quad (7-41c)$$

and it is shown plotted in Figure 7.13. The quadratic distribution is used to represent the phase variations at the aperture of a horn and of defocused (along the symmetry axis) reflector and lens antennas.

The space factor patterns corresponding to the phase distributions of (7-41a)–(7-41c) can be obtained by using (7-1). Because the analytical formulations become lengthy and complex, especially for the quadratic and cubic distributions, they will not be included here. Instead, a general guideline of their effects will be summarized [18], [19].

Linear phase distributions have a tendency to tilt the main beam of an antenna by an angle θ_0 and to form an asymmetrical pattern. The pattern of this distribution can be obtained by replacing the u (for uniform phase) in Table 7.1 by $(u - \theta_0)$. In general, the half-power beamwidth of the tilted pattern is increased by $1/\cos \theta_0$ while the directivity is decreased by $\cos \theta_0$. This becomes more apparent by realizing that

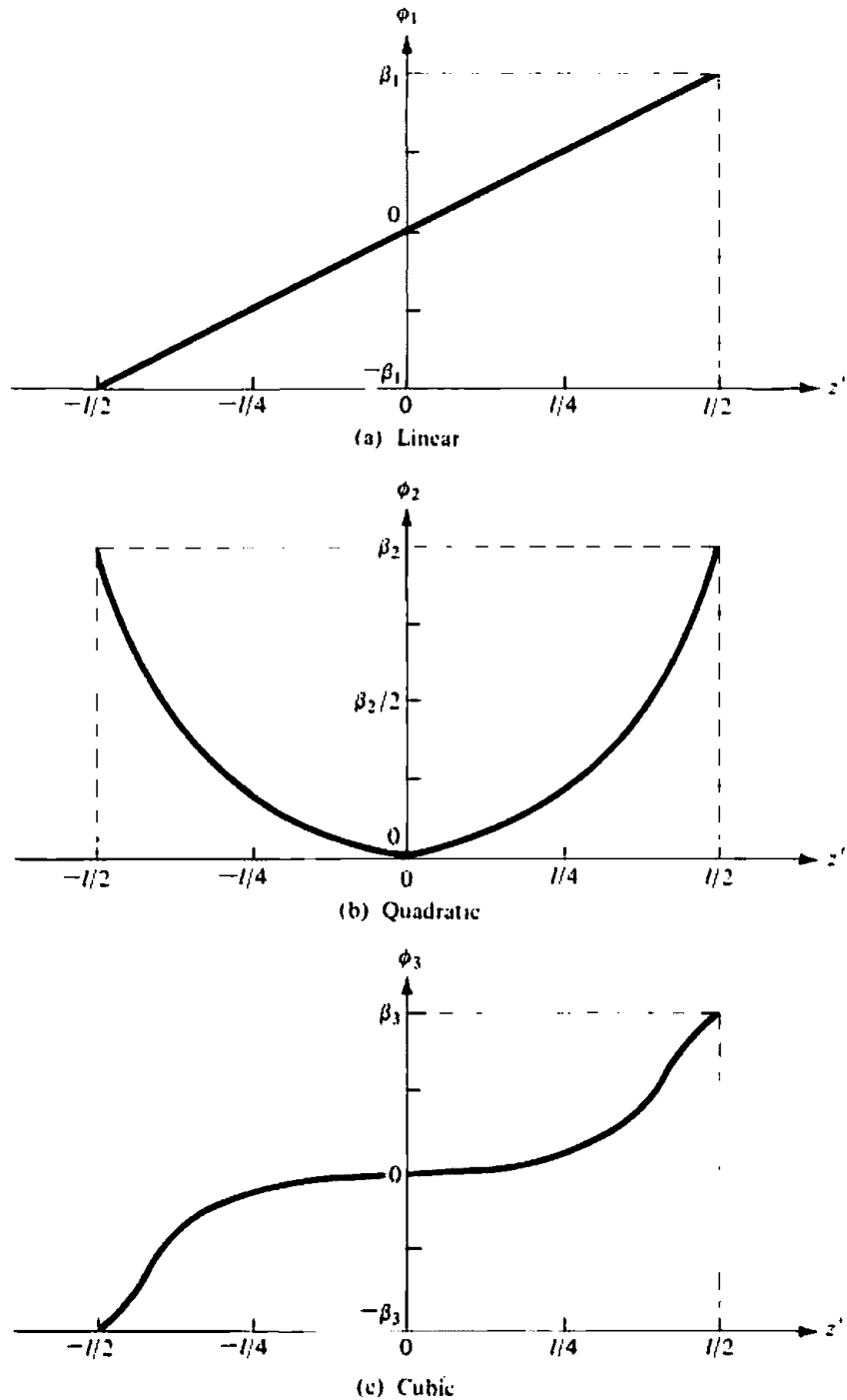


Figure 7.13 Linear, quadratic, and cubic phase variations.

the projected length of the line source toward the maximum is reduced by $\cos \theta_0$. Thus the effective length of the source is reduced.

Quadratic phase errors lead primarily to a reduction of directivity, and an increase in side lobe level on either side of the main lobe. The symmetry of the original pattern is maintained. In addition, for moderate phase variations, ideal nulls in the patterns disappear. Thus the minor lobes blend into each other and into the main beam, and they represent shoulders of the main beam instead of appearing as separate lobes. Analytical formulations for quadratic phase distributions were introduced in Chapter 13 on horn antennas.

Cubic phase distributions introduce not only a tilt in the beam but also decrease

the directivity. The newly formed patterns are asymmetrical. The minor lobes on one side are increased in magnitude and those on the other side are reduced in intensity.

7.10 CONTINUOUS APERTURE SOURCES

Space factors for aperture (two-dimensional) sources can be introduced in a similar manner as in Section 7.2.1 for line-sources.

7.10.1 Rectangular Aperture

Referring to the geometry of Figure 6.23(b), the space factor for a two-dimensional rectangular distribution along the x - y plane is given by

$$\text{SF} = \int_{-l_y/2}^{l_y/2} \int_{-l_x/2}^{l_x/2} A_n(x', y') e^{j(kx' \sin \theta \cos \phi + ky' \sin \theta \sin \phi + \phi_n(x', y'))} dx' dy' \quad (7-42)$$

where l_x and l_y are, respectively, the linear dimensions of the rectangular aperture along the x and y axes. $A_n(x', y')$ and $\phi_n(x', y')$ represent, respectively, the amplitude and phase distributions on the aperture.

For many practical antennas (such as waveguides, horns, etc.) the aperture distribution (amplitude and phase) is separable. That is,

$$A_n(x', y') = I_x(x') I_y(y') \quad (7-42a)$$

$$\phi_n(x', y') = \phi_x(x') + \phi_y(y') \quad (7-42b)$$

so that (7-42) can be written as

$$\text{SF} = S_x S_y \quad (7-43)$$

where

$$S_x = \int_{-l_x/2}^{l_x/2} I_x(x') e^{j(kx' \sin \theta \cos \phi + \phi_x(x'))} dx' \quad (7-43a)$$

$$S_y = \int_{-l_y/2}^{l_y/2} I_y(y') e^{j(ky' \sin \theta \sin \phi + \phi_y(y'))} dy' \quad (7-43b)$$

which is analogous to the array factor of (6-85)–(6-85b) for discrete-element arrays.

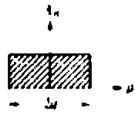


The evaluation of (7-42) can be accomplished either analytically or graphically. If the distribution is separable, as in (7-42a) and (7-42b), the evaluation can be performed using the results of a line-source distribution.

The total field of the aperture antenna is equal to the product of the element and space factors. As for the line sources, the element factor for apertures depends on the type of current density and its orientation.

7.10.2 Circular Aperture

The space factor for a circular aperture can be obtained in a similar manner as for the rectangular distribution. Referring to the geometry of Figure 6.32, the space factor for a circular aperture with radius a can be written as

Table 7.2 RADIATION CHARACTERISTICS FOR CIRCULAR APERTURES AND CIRCULAR PLANAR ARRAYS WITH CIRCULAR SYMMETRY AND TAPERED DISTRIBUTION

Distribution	Uniform	Radial Taper	Radial Taper Squared
Distribution (analytical)	$I_0 \left[1 - \left(\frac{\rho'}{a} \right)^2 \right]^0$	$I_1 \left[1 - \left(\frac{\rho'}{a} \right)^2 \right]^1$	$I_2 \left[1 - \left(\frac{\rho'}{a} \right)^2 \right]^2$
Distribution (graphical)			
Space factor (SF) $u = \left(2\pi \frac{a}{\lambda} \right) \sin \theta$	$I_0 2\pi a^2 \frac{J_1(u)}{u}$	$I_1 4\pi a^2 \frac{J_2(u)}{u}$	$I_2 16\pi a^2 \frac{J_3(u)}{u}$
Half-power beamwidth (degrees) $a \gg \lambda$	$\frac{29.2}{(a/\lambda)}$	$\frac{36.4}{(a/\lambda)}$	$\frac{42.1}{(a/\lambda)}$
First null beamwidth (degrees) $a \gg \lambda$	$\frac{69.9}{(a/\lambda)}$	$\frac{93.4}{(a/\lambda)}$	$\frac{116.3}{(a/\lambda)}$
First side lobe max. (to main max.) (dB)	-17.6	-24.6	-30.6
Directivity factor	$\left(\frac{2\pi a}{\lambda} \right)^2$	$0.75 \left(\frac{2\pi a}{\lambda} \right)^2$	$0.56 \left(\frac{2\pi a}{\lambda} \right)^2$

$$SF(\theta, \phi) = \int_0^{2\pi} \int_0^a A_n(\rho', \phi') e^{j[k\rho' \sin \theta \cos(\phi - \phi') + \zeta_n(\rho', \phi')]} \rho' d\rho' d\phi' \quad (7-44)$$

where ρ' is the radial distance ($0 \leq \rho' \leq a$), ϕ' is the azimuthal angle over the aperture ($0 \leq \phi' \leq 2\pi$ for $0 \leq \rho' \leq a$), and $A_n(\rho', \phi')$ and $\zeta_n(\rho', \phi')$ represent, respectively, the amplitude and phase distributions over the aperture. Equation (7-44) is analogous to the array factor of (6-112a) for discrete elements.

If the aperture distribution has uniform phase [$\zeta_n(\rho', \phi') = \zeta_0 = 0$] and azimuthal amplitude symmetry [$A_n(\rho', \phi') = A_n(\rho')$], (7-44) reduces, by using (5-48), to

$$SF(\theta) = 2\pi \int_0^a A_n(\rho') J_0(k\rho' \sin \theta) \rho' d\rho' \quad (7-45)$$

where $J_0(x)$ is the Bessel function of the first kind and of order zero.

Many practical antennas, such as a parabolic reflector, have distributions that taper toward the edges of the apertures. These distributions can be approximated reasonably well by functions of the form

$$A_n(\rho') = \begin{cases} \left[1 - \left(\frac{\rho'}{a} \right)^2 \right]^n & 0 \leq \rho' \leq a, \quad n = 0, 1, 2, 3, \dots \\ 0 & \text{elsewhere} \end{cases} \quad (7-46)$$

For $n = 0$, (7-46) reduces to a uniform distribution.

The radiation characteristics of circular apertures or planar circular arrays with distributions (7-46) with $n = 0, 1, 2$ are shown tabulated in Table 7.2 [19]. It is apparent, as before, that distributions with lower taper toward the edges (larger values of n) have smaller side lobes but larger beamwidths. In design, a compromise between side lobe level and beamwidth is necessary.

References

1. S. A. Schelkunoff, "A Mathematical Theory of Linear Arrays," *Bell System Technical Journal*, Vol. 22, pp. 80–107, 1943.
2. H. G. Booker and P. C. Clemmow, "The Concept of an Angular Spectrum of Plane Waves, and Its Relation to That of Polar Diagram and Aperture Distribution," *Proc. IEE* (London), Paper No. 922, Radio Section, Vol. 97, pt. III, pp. 11–17, January 1950.
3. P. M. Woodward, "A Method for Calculating the Field over a Plane Aperture Required to Produce a Given Polar Diagram," *J. IEE*, Vol. 93, pt. IIIA, pp. 1554–1558, 1946.
4. P. M. Woodward and J. D. Lawson, "The Theoretical Precision with Which an Arbitrary Radiation-Pattern May Be Obtained from a Source of a Finite Size," *J. IEE*, Vol. 95, Pt. III, No. 37, pp. 363–370, September 1948.
5. T. T. Taylor, "Design of Line-Source Antennas for Narrow Beamwidth and Low Side-lobes," *IRE Trans. Antennas Propagat.*, Vol. AP-3, No. 1, pp. 16–28, January 1955.
6. T. T. Taylor, "One Parameter Family of Line Sources Producing Modified $\text{Sin}(\pi u)/\pi u$ Patterns," *Hughes Aircraft Co. Tech. Mem. 324*, Culver City, Calif., Contract AF 19(604)-262-F-14, September 4, 1953.
7. R. S. Elliott, "On Discretizing Continuous Aperture Distributions," *IEEE Trans. Antennas Propagat.*, Vol. AP-25, No. 5, pp. 617–621, September 1977.
8. R. C. Hansen (ed.), *Microwave Scanning Antennas*, Vol. 1, Academic Press, New York, 1964, p. 56.
9. J. Ruze, "Physical Limitations on Antennas," MIT Research Lab., Electronics Tech. Rept. 248, October 30, 1952.
10. M. I. Skolnik, *Introduction to Radar Systems*, McGraw-Hill, New York, 1962, pp. 320–330.
11. R. S. Elliott, "Criticisms of the Woodward-Lawson Method," *IEEE Antennas and Propagation Society Newsletter*, Vol. 30, p. 43, June 1988.
12. H. Steyskal, "The Woodward-Lawson Method: A Second Opinion," *IEEE Antennas and Propagation Society Newsletter*, Vol. 30, p. 48, October 1988.
13. R. S. Elliott, "More on the Woodward-Lawson Method," *IEEE Antennas and Propagation Society Newsletter*, Vol. 30, pp. 28–29, December 1988.
14. H. Steyskal, "The Woodward-Lawson Method-To Bury or Not to Bury," *IEEE Antennas and Propagation Society Newsletter*, Vol. 31, pp. 35–36, February 1989.
15. H. J. Orchard, R. S. Elliott, and G. J. Stern, "Optimizing the Synthesis of Shaped Beam Antenna Patterns," *IEE Proceedings*, Part H, pp. 63–68, 1985.
16. R. S. Elliott, "Design of Line Source Antennas for Narrow Beamwidth and Asymmetric Low Sidelobes," *IEEE Trans. Antennas Propagat.*, Vol. AP-23, No. 1, pp. 100–107, January 1975.
17. G. N. Watson, *A Treatise on the Theory of Bessel Functions*, 2nd. Ed., Cambridge University Press, London, pp. 50 and 379, 1966.
18. S. Silver (ed.), *Microwave Antenna Theory and Design*, MIT Radiation Laboratory Series, Vol. 12, McGraw-Hill, New York, 1965, Chapter 6, pp. 169–199.

19. R. C. Johnson and H. Jasik (eds.), *Antenna Engineering Handbook*, 2nd. Ed., McGraw-Hill, New York, 1984, pp. 2-14 to 2-41.

PROBLEMS

- 7.1. A three-element array is placed along the z -axis. Assuming the spacing between the elements is $d = \lambda/4$ and the relative amplitude excitation is equal to $a_1 = 1$, $a_2 = 2$, $a_3 = 1$,
- find the angles where the array factor vanishes when $\beta = 0$, $\pi/2$, π , and $3\pi/2$
 - plot the relative pattern for each array factor
- Use Schelkunoff's method.
- 7.2. Design a linear array of isotropic elements placed along the z -axis such that the zeros of the array factor occur at $\theta = 0^\circ$, 60° , and 120° . Assume that the elements are spaced $\lambda/4$ apart and that the progressive phase shift between them is 0° .
- Find the required number of elements.
 - Determine their excitation coefficients.
 - Write the array factor.
 - Plot the array factor pattern to verify the validity of the design.
- 7.3. The z -plane array factor of an array of isotropic elements placed along the z -axis is given by

$$AF = z(z^4 - 1)$$

Determine the

- number of elements of the array. If there are any elements with zero excitation coefficients (null elements), so indicate
 - position of each element (including that of null elements) along the z axis
 - magnitude and phase (in degrees) excitation of each element
 - angles where the pattern vanishes when the total array length (including null elements) is 2λ
- 7.4. Repeat Prob. 7.3 when

$$AF = z(z^3 - 1)$$

- 7.5. Repeat Example 7.2 when

$$SF(\theta) = \begin{cases} 1 & 40^\circ \leq \theta \leq 140^\circ \\ 0 & \text{elsewhere} \end{cases}$$

- 7.6. Repeat the Fourier transform design of Example 7.2 for a line source along the z -axis whose sectoral pattern is given by

$$SF(\theta) = \begin{cases} 1 & 60^\circ \leq \theta \leq 120^\circ \\ 0 & \text{elsewhere} \end{cases}$$

Use $l = 5\lambda$ and 10λ . Compare the reconstructed patterns with the desired one.

- 7.7. Repeat the Fourier transform design of Problem 7.6 for a linear array with a spacing of $d = \lambda/2$ between the elements and
- $N = 11$ elements
 - $N = 21$ elements
- 7.8. Repeat the design of Problem 7.6 using the Woodward-Lawson method for line-sources.
- 7.9. Repeat the design of Problem 7.7 using the Woodward-Lawson method for linear arrays for $N = 10, 20$.
- 7.10. Design, using the Woodward-Lawson method, a line-source of $l = 5\lambda$ whose space factor pattern is given by

$$SF(\theta) = \sin^3(\theta) \quad 0^\circ \leq \theta \leq 180^\circ$$

Determine the current distribution and compare the reconstructed pattern with the desired pattern.

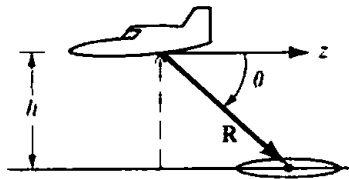
- 7.11. Repeat the design of Problem 7.10 for a linear array of $N = 10$ elements with a spacing of $d = \lambda/2$ between them.
- 7.12. In target-search, grounding-mapping radars, and in airport beacons it is desirable to have the echo power received from a target, of constant cross section, to be independent of its range R .

Generally, the far-zone field radiated by an antenna is given by

$$|E(R, \theta, \phi)| = C_0 \frac{|F(\theta, \phi)|}{R}$$

where C_0 is a constant. According to the geometry of the figure

$$R = h/\sin(\theta) = h \csc(\theta)$$



For a constant value of ϕ , the radiated field expression reduces to

$$|E(R, \theta, \phi = \phi_0)| = C_0 \frac{|F(\theta, \phi = \phi_0)|}{R} = C_1 \frac{|f(\theta)|}{R}$$

A constant value of field strength can be maintained provided the radar is flying at a constant altitude h and the far-field antenna pattern is equal to

$$f(\theta) = C_2 \csc(\theta)$$

This is referred to as a cosecant pattern, and it is used to compensate for the range variations. For very narrow beam antennas, the total pattern is approximately equal to the space or array factor. Design a line-source, using the Woodward-Lawson method, whose space factor is given by

$$SF(\theta) = \begin{cases} 0.342 \csc(\theta), & 20^\circ \leq \theta \leq 60^\circ \\ 0 & \text{elsewhere} \end{cases}$$

Plot the synthesized pattern for $l = 20\lambda$, and compare it with the desired pattern.

- 7.13. Repeat the design of Problem 7.12 for a linear array of $N = 41$ elements with a spacing of $d = \lambda/2$ between them.
- 7.14. For some radar search applications, it is more desirable to have an antenna which has a square beam for $0 \leq \theta \leq \theta_0$, a cosecant pattern for $\theta_0 \leq \theta \leq \theta_m$, and it is zero elsewhere. Design a line-source, using the Woodward-Lawson method, with a space factor of

$$SF(\theta) = \begin{cases} 1 & 15^\circ \leq \theta < 20^\circ \\ 0.342 \csc(\theta) & 20^\circ \leq \theta \leq 60^\circ \\ 0 & \text{elsewhere} \end{cases}$$

Plot the reconstructed pattern for $l = 20\lambda$, and compare it with the desired pattern.

- 7.15. Repeat the design of Problem 7.14, using the Woodward-Lawson method, for a linear array of 41 elements with a spacing of $d = \lambda/2$ between them.
- 7.16. Design a Taylor (Tschebyscheff error) line-source with a
 (a) -25 dB side lobe level and $\bar{n} = 5$
 (b) -20 dB side lobe level and $\bar{n} = 10$
 For each, find the half-power beamwidth and plot the normalized current distribution and the reconstructed pattern when $l = 10\lambda$.
- 7.17. Derive (7-33) using (7-1), (7-32), and Gegenbauer's finite integral and polynomials.

- 7.18. Repeat the design of Example 7.7 for an array with $l = 4\lambda$, $d = \lambda/2$, $N = 9$.
- 7.19. Design a broadside five-element, -40 dB side lobe level Taylor (one-parameter) distribution array of isotropic sources. The elements are placed along the x -axis with a spacing of $\lambda/4$ between them. Determine the
- (a) normalized excitation coefficients (amplitude and phase) of each element
 - (b) array factor
- 7.20. Derive the space factors for uniform, triangular, cosine, and cosine squared line-source continuous distributions. Compare with the results in Table 7.1.
- 7.21. Compute the half-power beamwidth, first null beamwidth, first side lobe level (in dB), and directivity of a linear array of closely spaced elements with overall length of 4λ when its amplitude distribution is
- (a) uniform (b) triangular
 - (c) cosine (d) cosine squared
- 7.22. Derive the space factors for the uniform radial taper, and radial taper-squared circular aperture continuous distributions. Compare with the results in Table 7.2.
- 7.23. Compute the half-power beamwidth, first null beamwidth, first side lobe level (in dB), and gain factor of a circular planar array of closely spaced elements, with radius of 2λ when its amplitude distribution is
- (a) uniform
 - (b) radial taper
 - (c) radial taper-squared